New quantitative analyses of the *Nacholapithecus kerioi* proximal ulna confirm morphological affinities with *Equatorius* and large papionins

Running title: *Nacholapithecus* ulna quantitative analysis

Marta Pina[1,2*], Masato Nakatsukasa[3]

[1] *South Bank Applied BioEngineering Research (SABER), School of Engineering, London South Bank University, London SE1 0AA, UK.*

[2§] *Institut Català de Paleontologia Miquel Crusafont, Universitat Autònoma de Barcelona, c/ Columnes s/n, Campus de la UAB, 08193 Cerdanyola del Vallès, Barcelona, Spain. marta.pina@icp.cat*

[3] *Laboratory of Physical Anthropology, Graduate School of Science, Kyoto University, Kyoto 606-8502, Japan. nakatsuk@anthro.zool.kyoto-u.ac.jp*

*Corresponding author:

E-mail address: marta.pina@icp.cat (M. Pina)

[§] Present institution

Abstract

Objectives

The elbow of *Nacholapithecus* has been extensively described qualitatively, however its ulnar morphology has never been the focus of an in-depth quantitative analysis before. Hence, our main aim is quantifying the proximal ulnar morphology in *Nacholapithecus* and exploring whether it is similar to those of *Equatorius* and *Griphopithecus* as previously reported.

Materials and Methods

We compared *Nacholapithecus* proximal ulnar morphology with a sample of extant and extinct anthropoids through principal component analysis and agglomerative hierarchical cluster analysis. Moreover, we calculated the Cophenetic Correlation Coefficient and checked for taxonomical group mean differences through MANOVA and pairwise post-hoc comparisons, as well as the phylogenetic signal in the variables used.

Results

The *Nacholapithecus* ulna displays a moderately long and relatively narrow olecranon, a relatively wide trochlear surface-radial notch width, and a relatively thin sigmoid notch depth. These features resemble those of large papionins and chimpanzees, and some extinct taxa, mainly *Equatorius*.

Discussion

Results presented here reinforce previous inferences on the functional morphology of the *Nacholapithecus* elbow, showing adaptations for general quadrupedal behaviors. However, other derived features (e.g., a relatively wide trochlear surface) might be associated with the ape-like traits described for its distal humerus (e.g., wide trochlear groove), thus displaying a combination of primitive and derived features in the proximal

ulna. Finally, affinities with large papionins could suggest the presence of some terrestrial habits in *Nacholapithecus*. However, the lack of evidence in the rest of the skeleton prevents us from suggesting terrestrial affinities in this taxon in a conclusive manner.

Keywords

Elbow, functional morphology, hominoids, Miocene, Kenya

Research Highlights

- Quantitative analyses of the *Nacholapithecus* proximal ulna support resemblances with large papionins and *Equatorius*.
- Results suggest some functional similarities with terrestrial papionins combined with derived hominoid-like traits.

Introduction

The elbow is one of the most diagnostic joints among hominoids, which share a suite of traits at the humeroulnar, humeroradial and proximal radioulnar joints related to the stability of the whole elbow during flexion-extension movements and the ability of pronation-supination of the forearm (Rose, 1988, 1997). Some of these features include a wide groove and spool-shaped trochlea in the humerus with a deep zona conoidea, a short ulnar olecranon with a keeled trochlear notch, and a rounded and laterally beveled radial head (Rose, 1988, 1993; Drapeau, 2008; Alba, Moyà-Solà & Almécija, 2011; Arias-Martorell, Urciuoli, Almécija, Alba & Nakatsukasa, 2023). This complex of features has also been associated with the increasing acquisition of antipronograde locomotor modes through the evolution of the superfamily Hominoidea (apes and humans), which rely on an extensive use of the forelimb over the hind limb (except in the case of humans) (Richmond, Fleagle, Kappelman & Swisher, 1998).

The proximal ulna is an important component of the elbow complex and extant hominoids share a set of derived traits such as distally wide and keeled trochlear notch, short olecranon process, and an anteriorly projected coronoid process (humans are exceptions for some of these traits, for instance showing a less keeled notch and a longer olecranon; e.g., Rose, 1988; Richmond et al., 1998; Drapeau, 2004, 2008). The functional significance of these traits has been explored differently. For example, Drapeau (2004) investigated the functional morphology of olecranon length and orientation in anthropoids, suggesting that variation in this trait is limited, with only suspensory primates deviating from the general pattern. In any case, variation in olecranon morphology affects the extension of the elbow (i.e., leverage of the forelimb extensor muscles), since changes in its length and orientation influence the moment arm of the triceps brachii muscle (Fleagle, Simons & Conroy, 1975; Rose, 1993; Drapeau,

2004; Rein, Harrison & Zollikofer, 2011). The breadth of the trochlear notch and the presence of a keel running proximodistally are traits also related to the stabilization of the elbow and the enhancement of hominoid rotation capabilities (Fleagle et al., 1975; Rose, 1988). The keel itself has been related to the forces generated during arboreal locomotion, so that this structure would help to better resist mediolateral loads in more arboreal taxa (e.g., *Pongo*; Schmitt, 2003; Drapeau, 2008). Likewise, the morphology of the radial notch in hominoids has been also associated with increasing mobility of the elbow for supination and pronation (Fleagle et al., 1975; Rose, 1983; Richmond et al., 1998).

Within the fossil record, Early-Middle Miocene African apes show an overall primitive configuration of the proximal ulna associated with quadrupedal behaviors (Alba, Almécija, Casanovas-Vilar, Méndez & Moyà-Solà, 2012; Takano et al., 2020). Particularly, *Proconsul* and *Ekembo* (family Proconsulidae), and *Equatorius* and *Nacholapithecus* (family Afropithecidae) share, in general terms, a narrow trochlear notch, absence or only faint development of a median keel, a proximally protruded olecranon, an anteriorly projected coronoid process, and a deep shaft (Richmond et al., 1998; Alba et al., 2012; Takano et al., 2020; taxonomy used in this work follows Urciuoli & Alba, 2023). On the other hand, younger apes from the Late Miocene of Eurasia like *Oreopithecus*, *Hispanopithecus*, and *Danuvius* already show a more derived (extant ape-like) morphology of the proximal ulna, with a wider trochlear notch, markedly developed keel, shorter olecranon process, and an anteriorly projected coronoid process (e.g., Harrison, 1986; Drapeau, 2008; Alba et al., 2012; Böhme et al., 2019).

Nacholapithecus kerioi is an afropithecid (subfamily Equatorinae) from northern Kenya (ca. 16-15 Ma, Aka Aiteputh Formation, Samburu County; Nakatsukasa,

Yamanaka, Kunimatsu, Shimizu & Ishida, 1998; Sawada et al., 1998; Ishida, Kunimatsu, Nakatsukasa & Nakano, 1999; Nakatsukasa and Kunimatsu, 2009). The postcranial skeleton of this species is well-represented. The holotype (KNM-BG 35250) was described in 2004 and represents one of the most complete Miocene hominoid skeletons in the fossil record (Ishida, Kunimatsu, Takano, Nakano & Nakatsukasa, 2004). In addition, continuous field campaigns through the years have provided numerous fossils of other individuals (see some examples in Kikuchi et al., 2018; Takano et al., 2020; Pina et al., 2021). Among these remains, the elbow region, particularly the proximal ulna, is well-represented (Ishida et al., 2004; Takano et al., 2018, 2020; see also Arias-Martorell et al., 2023 for a quantitative study on the radial head). Whereas the overall ulnar morphology of *Nacholapithecus* resembles those of other afropithecids (*Equatorius*) and kenyapithecines (*Griphopithecus*), it shows some distinctive features that distinguish it from older African taxa, such as *Ekembo* or *Turkanapithecus*, by displaying a flat and laterally facing radial notch and a wider and more anteriorly directed coronoid process (Rose, Nakano & Ishida, 1996; Ishida et al., 2004; Takano et al., 2018, 2020). Another distinctive feature of *Nacholapithecus* is that this taxon might have relatively large forelimbs related to the hind limbs (Ishida et al., 2004; Nakatsukasa and Kunimatsu, 2009).

Although the elbow of *Nacholapithecus* has been extensively described elsewhere, hitherto the morphology of the proximal ulna of this taxon has not been quantified in-depth owing to a scarcity of suitable specimens. However, the recent addition of better-preserved fossils ameliorated this problem (see Takano et al., 2020). In particular, Nishimura and colleagues (Nishimura, Russo, Nengo & Miller, 2022) incorporated KNM-BG 38391B in their work focused on the KNM-WS 65401 proximal ulnar fragment from Buluk (Kenya), providing preliminary quantitative results about the

affinities of the *Nacholapithecus* ulna. The present study focuses on providing new linear measurements and body mass estimates for the proximal ulna of *Nacholapithecus* (some of them considering morphological aspects that were not covered in Nishimura et al., 2022's analysis), quantitatively comparing its morphology with other extinct and extant catarrhines, exploring its cophenetic affinities with the selected sample, provide new body mass estimates and, ultimately, inferring locomotor affinities for this taxon. More specifically, we aim to test whether the ulna of *Nacholapithecus* is like that of *Equatorius* and *Griphopithecus* not only qualitatively (Takano et al., 2018), but also in quantitative terms. Thus, we hypothesize that the proximal ulnar morphology of *Nacholapithecus* will be similar to those of extant taxa that habitually navigate arboreal settings by using quadrupedal behaviors, such as arboreal cercopithecoids. Additionally, previous works have highlighted the distorted nature of the holotype elements (e.g., Nakatsukasa and Kunimatsu, 2009). Specifically, differences between the holotype (KNM-BG 35250) and other isolated remains have been demonstrated for the femora (Pina et al., 2021). Here, we qualitatively and quantitatively compare the left ulna of the KNM-BG 35250 skeleton with another proximal ulnar fragment that does not show significant plastic deformation (KNM-BG 38391B), and we test whether the distinctiveness (e.g., radial notch morphology) of the *Nacholapithecus* proximal ulna is real or just related to taphonomic effects (see Pina et al., 2021 for discussion on this topic in relation to the proximal femoral end). In this regard, we expect that KNM-BG 38391B will show some shape differences compared with the KNM-BG 35250 ulnae. Finally, the analysis of undistorted fossils also allows us to calculate the body mass in *Nacholapithecus*, using KNM-BG 38391B, and compare our estimates with those provided in previous works.

Material and Methods

Sample

A total of five proximal ulnar fragments of *Nacholapithecus* have been measured in this study, including the right and left fragments of the species holotype and those specimens previously published by Takano and colleagues (Ishida et al., 2004; Takano et al., 2018, 2020; Table 1). However, KNM-BG 35250C and KNM-BG 38391B were the only specimens complete enough for all 16 linear variables to be measured (see below and Table 2). The latter specimen mostly preserves the original form despite minor weathering (Takano et al., 2020: Figure 4). In the case of the holotype specimens, the olecranon is compressed mediolaterally and the radial notch is flattened in KNM-BG 35250C (left ulna); whereas KNM-BG 35250V (right ulna) displays a broken olecranon process (anteroproximal region) and sigmoid notch (proximal part), and the proximal shaft is mediolaterally flattened (Takano et al., 2018). As this damage could affect the results, the reliability of KNM-BG 35250C for morphological comparisons is discussed in the Discussion section below. Additionally, we combined reliable or less-affected measurements from KNM-BG 35250C and KNM-BG 35250V to create a combined specimen (referred to as *KNM-BG 35250com*) for the analysis (we took KNM-BG 35250C as a base and added reliable measurements from KNM-BG 35250V when those were tentative in the former to reach the set of 16 variables; Table 1).

Nacholapithecus ulnae were compared with a sample of extant anthropoids listed in Table 3. Measurements from these specimens were collected at the American Museum of Natural History (AMNH, New York, USA). Furthermore, additional ulnae of extinct taxa were incorporated in the analyses: *Epipliopithecus vindobonensis* (NHMW1970/1397/0020; Zapfe, 1960); *Equatorius africanus* (KNM-TH 28860K;

Sherwood et al., 2002); *Turkanapithecus kalakolensis* (KNM-WK 16950R; Leakey, Leakey & Walker, 1988); *Griphopithecus darwini* (KF 1992/581; Begun, 1992); and *Hispanopithecus laietanus* (IPS34575g; Alba et al., 2012). Although the Miocene hominoid fossil record includes some other taxa with available proximal ulnae (e.g., KNM-RU 1786 attributed to *Ekembo nyanzae*), they were not included here because it was not possible to take all the measurements listed in Table 2. Measurements of the *Nacholapithecus* specimens, KNM-WK 16950R, NHMW1970/1397/0020, and IPS34575g were taken on the original fossils in the National Museums of Kenya (NMK, Kenya), Naturhistorisches Museum Wien (NHM, Austria), and the Institut Català de Paleontologia Miquel Crusafont (ICP, Spain), respectively. Measurements of KNM-TH 28860K and KF 1992/581 were collected from a 3D model (generated with a NextEngine scanner) and a cast, respectively.

Body mass estimation

Even though the hominoid status of *Nacholapithecus* is widely supported (e.g., see Alba, 2012, Kunimatsu, Nakatsukasa, Shimizu, Nakano & Ishida, 2019, Pugh, 2022; Urciuoli & Alba, 2023), its general postcranial morphology does not completely fit that of extant hominoids nor that of cercopithecoids, showing a mosaic combination of traits (see Discussion). For this reason, body mass (BM) was estimated using the allometric BM prediction equations provided by Ruff (2003) for both extant hominoids (sex/species means): lnBM (kg) = 1.314*lnUTSA-5.101; and extant catarrhines (sex/species means of cercopithecoids and hominoids): lnBM = 1.194*lnUTSA-4.225. UTSA (ulnar trochlear surface area in mm^2) is used as a BM estimator and is calculated as follows: UTSA = NPD*TAB*acos(1-((2*UTDP)/NPD)), where UTDP = depth of the trochlear notch (measured as the average of the three depths taken perpendicular to

and from the midpoint of NPD, to the medial and lateral surface boundaries and to the middle of the trochlear notch; see Table 2 for NPD and TAB definitions and Ruff, 2002 for further information). A correction factor for the detransformation bias was applied (multiplying the factor by the raw BM estimate obtained from the equations), based on the quasimaximum likelihood estimator (QMLE): QMLE = $\exp(SEE^2/2)$, where SEE = standard error of the estimate (Ruff, 2003). Given that most of the *Nacholapithecus* ulnar specimens are not complete, only KNM-BG 38391B (UTDP = 10.97 mm) was used to estimate the species BM using UTSA. Unfortunately, the shaft is not well-preserved in the *Nacholapithecus* ulnar fragments, and estimations of the BM through midshaft measurements could not be performed.

Measurements and statistical analysis

Fifteen linear measurements extracted from Richmond et al. (1998) were taken on the proximal end of the ulnae for extant anthropoids and fossil fragments and measured using a digital calliper to the nearest 0.1 mm. In addition, one extra measurement (OLP) was taken to quantify the length of the olecranon. OLP was taken from photographs with ulnae in lateral view and using the software Fiji version 2.0 (Schindelin et al., 2012). To take this measurement, the ulnae were first placed on the surface in a fully supinated position (i.e., the anterior anatomical side facing upwards), and then rotated 90 degrees (left or right depending on the side to which the ulna belonged). All 16 measurement definitions are listed and described in Table 2 and illustrated in Figure 1.

In order to remove size-related effects in the analysis, the overall proximal ulna size was calculated as the geometric mean (GM) of the 16 measurements (GM16). The ratio between each variable and GM16 was calculated and then log-transformed (natural

logarithms, ln) to obtain dimensionless Mosimann shape variables (Mosimann, 1970; Jungers, Falsetti & Wall, 1995).

Phylogenetic signal of the Mosimann variables -ln(Variable/GM16)- and lnGM16 was calculated through the Blomberg's K (the statistical significance was evaluated with the permutation test with 1,000 iterations; Blomberg, Garland & Ives, 2003) and Pagel's λ statistics (Pagel, 1999), under a Brownian motion model of evolution. The phylogenetic tree used as the base for both cases is a consensus and time-scaled (chronometric) phylogeny obtained from the 10kTrees Website (https://10ktrees.nunn-lab.org). These trees are based on genes available at GenBank (11 mitochondrial and 6 autosomal; Arnold, Matthews & Nunn, 2010).

Principal component analysis (PCA) of the Mosimann shape variables and lnGM16 were performed to explore major patterns of shape variation. To check for the cophenetic affinities of the taxonomic groups and fossils included in the analysis (Sokal and Rohlf, 1962), the PC score means per genera were calculated for PCs 1-3 and, together with the extinct taxa, dendrograms were built through agglomerative hierarchical cluster analysis, using the unweighted pair-group average (UPGMA) algorithm. The Cophenetic Correlation Coefficient (CPCC) was computed for each dendrogram to measure the goodness of the clustering's fit between the cophenetic distances and the original Euclidean distances of the computed matrix (Farris, 1969). Additionally, the Mosimann variables with the highest loadings in the PCA analyses were depicted in boxplots to visually compare between groups. After testing for normality (Shapiro-Wilk test), statistical differences between groups were inspected using the PC scores. Given that PC1-PC3 do not show a normal distribution ($p < 0.05$), a Kruskal-Wallis non-parametric test was used to check for group differences. Pairs of PCs were compared through permutational MANOVAs (non-parametric MANOVA)

and specific differences between groups were computed through pairwise post hoc multiple comparisons (BH –Benjamini-Hochberg– correction).

Finally, a PAB/GM16 vs TAB/GM16 scatter plot was also computed to visualize how PAB (proximal articular breadth of radial notch and trochlea) and TAB (trochlear articular breadth) relate and how groups are characterized by this index (i.e., relative mediolateral breadth of the coronoid process). These two measurements were selected because the width of the coronoid process has been frequently used to differentiate monkeys and apes (e.g., Rose, 1988 and Nishimura et al., 2022).

Analyses were performed with the statistical environment R v 4.2.1 through RStudio v 2022.07.0 GUI (R Core Team, 2022).

Results

Body mass estimations

The BM for KNM-BG 38391B after UTSA is estimated at 26.49±1.11 kg and 29.89±1.19 kg on the basis of allometric equations for extant hominoids and catarrhines, respectively (Table 4).

Shape comparisons

Values for the linear measurements taken for the *Nacholapithecus* specimens are listed in Table 1. Except PAP, the rest of variables show a significant phylogenetic signal when analyzed through the Pagel's λ statistic (Table 5). For those variables with a significant phylogenetic signal, a $\lambda > 0.7$ value was found for most of them (except in the case of RPD, whose $\lambda = 0.484$). The Blomberg's K metric is not significant for PSML, PAH, LAH, RPD, PAP, and OLP. Values for K are in all instances lower than 1 (Table 5).

PCA plots show the major patterns of shape variation for the 16 variables and the GM16 (Figure 2 and Figure S1). PC1 (38.2% of variance) is correlated with PAB and TAB positively, and OLP negatively; whereas PC2 (22.9% of variance) is correlated with NPD and RPD positively and SND negatively (Table 6). When plotting PC1 versus PC2 (Figure 2), both gorillas and orangutans are clearly separated from the rest of the anthropoid groups showing high PC1 scores and intermediate to low PC2 scores. Their high PC1 scores are due to a combination of relatively wide PAB and TAB, and shorter OLP (see also below and Figures 3A, B and 4C, respectively). Hylobatids also occupy their own morphospace showing high PC1 and PC2 scores (with some overlapping with *Ateles*). This group is separated from great apes along PC2 due to a relatively long NPD and RPD (Figure 3C, D) and a relatively thin SND (Figure 4A). Chimpanzees and papionins (mandrils and baboons) occupy their own morphospace showing low PC1 and PC2 scores. They are somewhat overlapping in PC1, but papionins generally have lower PC1 scores. Papionins display clearly narrower TAB (Figure 3A); and longer OLP (Figure 4C). Regarding PAB, they are intermediate while baboons show higher values among monkeys (Figure 3B). Furthermore, chimpanzees, papionins, and gorillas display a relatively thick SND (Figure 4A), which contributes to their low PC2 scores. Smaller monkeys (*Cercopithecus* and platyrrhines) and hylobatids are distinguished by their relatively thin SND (even though they clearly overlap with orangutans and somewhat with gorillas in PC2; Figure 4A); whereas only the *Ateles* morphospace overlaps with that of *Hoolock* and *Hylobates* in PC1, showing a trend towards a relatively shorter OLP (Figure 4C) and wider TAB and PAB (Figure 3A, B). Differences in PC3 (7.2% of the variance; Figure S1A, B) are less clear, although this axis aids to separate African apes

from Asian apes to some extent; and *Aloutta* from the rest of monkeys, although there is some overlap with the *Lagothrix* and *Ateles* morphospaces.

Differences among genera of extant catarrhines are statistically significant in all three PCs (PC1: chi-square = 105.46, $p < 0.001$; PC2: chi-square = 102.96, $p < 0.001$; PC3: chi-square = 81.17, $p < 0.001$). In addition, when PC-pairs are compared, differences among groups are also significant (PC1-2: F = 85.50, $p < 0.01$; PC1-3: F = 81.30, $p < 0.01$; PC2-3: F = 39.08, $p < 0.01$; see Table S1 for specific pairwise post hoc differences between genera).

Regarding *Nacholapithecus* and the rest of the extinct taxa, KNM-BG 38391B falls within the morphospace variation of papionins (specifically *Papio*) and is close to chimpanzees, by showing a relatively long OLP and relatively thick SND (Figures 2 and 4A, C). KNM-BG 35250C (the holotype) falls closer to the papionin morphospace and is characterized by a relatively narrow coronoid process, for both TAB and, mainly, PAB (Figure 3A, B). For the other two PCs (PC2 and PC3), both *Nacholapithecus* ulnae overlap with chimpanzees, large papionins and gorillas in PC2, and with non-*Cebus* platyrrhines, great apes and siamangs in PC3 (Figure 2 and Figure S1A, B). Finally, the *Nacholapithecus* combined specimen (*KNM-BG 35250com*) follows the same trend as the original *Nacholapithecus* fragments, occupying a somewhat intermediate position between them in PC1 and overlapping with the large papionins morphospace in the PC1-PC2 plot (Figure 2), with that of *Ateles* in the PC3-PC1 plot (Figure S1A), and with morphospaces of African great apes in the PC3-PC2 plot (Figure S1B). Compared to other fossil taxa (Figure 2), *Nacholapithecus* specimens falls close to *Equatorius* (especially *KNM-BG 35250com*) and *Hispanopithecus* (especially KNM-BG 38391B), and clearly departs from *Epipliopithecus* (which falls within the morphospace of small monkeys, in particular *Alouatta*), *Turkanapithecus* (which clearly departs from

hylobatids, but overlaps with the rest of groups in some way in both PC1 and PC2), and *Griphopithecus* in some extent (overall more similar to chimpanzees, *Ateles*, and large papionins).

An UPGMA dendrogram (Figure 5 and Figure S1C, D) allows visualization of how taxa are clustered on the basis of cophenetic similarities. The highest CPCC is found for PC1-PC2 (CPCC = 0.87; Figure 5). In this dendrogram, extant apes (except chimpanzees) are grouped together (*2*; node numbers after Figure 5), distinguishing between great apes (*Gorilla* and *Pongo*; *19*) and hylobatids (*18*; organized in two separated subclusters: *Hylobates-Hoolock* and *Symphalangus*). The other big cluster (*1*) is divided into two subclusters (*3* and *4*), with *Nacholapithecus* specimens, *Equatorius*, *Hispanopithecus,* and large papionins grouped in the same subcluster (*5*). *Griphopithecus* and chimpanzees form their own subcluster (*6*). Within *5*, KNM-BG 35250C is placed at the base, and KNM-BG 38391B is grouped with *Hispanopithecus* (*9*), and *KNM-BG 35250com* is grouped with *Equatorius* (*11*) and papionins (*8*). On the other hand, *Turkanapithecus* and *Epipliopithecus* are clustered together with the small cercopithecoids and the platyrrhine monkeys (*4*). The former (KNM-WK 16950R) is subgrouped with *Ateles* (*12*); *Epipliopithecus* is subclustered with the atelids *Alouatta* and *Lagothrix* (*15*). Dendrograms for the other two PC pairs (PC1-3 and PC2-3; Figure S1C, D) show some differences. For PC1-3, *Nacholapithecus* is grouped in a cluster with platyrrhines (but *Cebus*), chimpanzees, and the rest of the extinct taxa, except *Griphopithecus* and *Hispanopithecus* (CPCC = 0.83; Figure S1C). In the case of PC2-3, *Nacholapithecus* is clustered together with African great apes and *Equatorius* (CPCC = 0.76; Figure S1D). Contrarily to what could be expected, the three specimens of *Nacholapithecus* included in the analyses are not grouped immediately next to each

other in any of the three dendrograms and, in particular, they are clearly separated far from orangutans and hylobatids (Figure 5 and Figure S1C, D).

Finally, the (PAB/GM16)/(TAB/GM16) index shows that extant apes display relatively wide breadths of the radial notch-trochlear articular surface complex, showing especially a relatively wide TAB (Figure 6). KNM-BG 35250C clearly departs from the general trend in the sample, showing an index close to 1 and possessing the lowest value for PAB/GM16 among the whole sample (see Discussion). KNM-BG 38391B, the best-preserved *Nacholapithecus* specimen, shows similarities with *Ateles* for this region of the ulna and falls close to *Griphopithecus*. The combined specimen (*KNM-BG 35250com*) also shows a low value for PAB/GM16 (although not as extreme as KNM-BG 35250C) and falls closest to chimpanzees (Figure 6). The rest of the fossil ulnae display affinities with monkeys, except for *Hispanopithecus*, which clearly falls within the range of variation of chimpanzees; and *Griphopithecus*, whose value falls in an intermediate position between the morphospaces of chimpanzees and atelids (Figure 6).

Discussion

Body mass

Our estimated mean BM for *Nacholapithecus* (26.49 kg and 29.88kg using allometric equations for extant hominoids and catarrhines, respectively) based on the proximal ulna KNM-BG 38391B is notably higher compared to the 16.5 kg previously calculated from the proximal femur KNM-BG 38391A, found in association with the ulnar fragment and almost certainly belonging to the same individual (Kikuchi et al., 2018; Takano et al., 2020). However, our estimates are similar to others obtained based on the same ulna (KNM-BG 38391B): 26.14 kg (Nishimura et al., 2022); and based on

forelimb elements (ulnae, KNM-BG 38391B and KNM-BG 35250C; and humerus, KNM-BG 38384): 27 kg (Kikuchi, 2023).

While the available fossil evidence does not allow a direct calculation of the body proportions (limb lengths) in *Nacholapithecus*, the allometric scaling of the humeral distal epiphysis articular width vs the height of the proximal femur revealed that the forelimb was proportionally larger than the hind limb (Ishida et al., 2004; Nakatsukasa and Kunimatsu, 2009). The antebrachial remains (proximal ulna and radius) also follow this trend, which has been identified as a unique trait for this taxon (not shared with *Equatorius* and *Ekembo*; McCrossin, 1994; McCrossin and Benefit, 1997; Ishida et al., 2004). Given that it has been suggested that the forelimb would be proportionally larger than the hind limb in *Nacholapithecus*, the most plausible explanation for our BM results may relate to these limb proportions, suggesting that the BM obtained from the ulna tends to overestimate the mass of this extinct taxon or, at least, to produce larger BMs than those estimated based on hind limb elements. Additionally, Ruff (2003) suggested that the ulna (through UTSA) is usually a poorer BM predictor than the femur and the tibia and, therefore, estimations obtained from those bones may be favored.

KNM-BG 38391A has been attributed to a male individual (Kikuchi et al., 2018). Following our estimated BM range based on the proximal ulna (~26-30 kg), *Nacholapithecus* would be similar in size to large papionin males such as *Papio anubis* (25.1 kg), *Mandrillus sphinx* (31.6 kg) or *Papio ursinus* (29.8 kg; BMs of extant taxa after Smith and Jungers, 1997). However, all the evidence together provides an average BM of 22.7 kg (Kikuchi, 2023), and thus *Nacholapithecus* could have been intermediate in size between the former examples and smaller papionins, such as *Papio hamadryas* (16.9 kg) or *Theropithecus gelada* (19 kg; BM by Smith and Jungers, 1997).

Proximal ulnar shape

The proximal ulna of *Nacholapithecus* displays a moderately long olecranon, an extensive proximolateral articular extension and non-keeled sigmoid notch, an anteriorly projected coronoid process, a wide and moderately concave coronoid process superior surface, a small and laterally faced radial notch, an anteroposteriorly thick proximal shaft, and a deep groove for the insertion of the muscle brachialis (Nakatsukasa et al., 1998; Ishida et al., 2004; Takano et al., 2018, 2020). We quantitatively record some of these features in our analysis, which includes an intermediate-to-high SND and OLP. These characteristics are also present in *Papio* and *Mandrillus* (Figure 4A, C). Apart from those traits, papionins algo show a long olecranon process and a non-deep epiphysis. Such features are related to the leverage enhancement of the muscle triceps brachii and the elbow hyperextension prevention during quadrupedal terrestrial locomotion (Richmond et al., 1988; Rose, 1993; Drapeau, 2004; Nishimura et al., 2022). Nonetheless, papionins differ from *Nacholapithecus* in showing a retroflexed olecranon, which results in a posteriorly expanded process (and other traits like the more proximally oriented radial notch; Richmond et al., 1988). Unfortunately, the conventional linear dimensions adapted here do not recover the potential retroflexion (i.e., orientation) or expansion of the olecranon itself, so that the comparisons between *Nacholapithecus* and large papionins are purely qualitative and limited in this regard. In fact, *Nacholapithecus*' non-retroflexed olecranon process is more similar to that of smaller cercopithecids like *Cercopithecus* or *Nasalis* (see Ishida et al., 2004 and Takano et al., 2020). Our qualitative observations are supported by the results obtained by Nishimura et al. (2022), whose 3D geometric morphometric analysis better recovers this trait. Their results place *Nacholapithecus*' proximal ulnar morphology within the cercopithecoid morphospace, showing closer affinities with the

smaller taxa (i.e., *Cercopithecus* sp., *Chlorocebus* sp., *Macaca fascicularis*, and *Presbytis* spp.) in their sample.

We also register that *Nacholapithecus* displays a relatively narrow mediolateral articular breadth (PAB), but a relatively wide trochlear mediolateral breath (TAB), as in spider monkeys and chimpanzees (Figures 3A, B and 6). Figure 6 also shows that the configuration of this complex (radial notch-trochlear articular surface breadths) in KNM-BG 35250C clearly departs from the general pattern of the whole sample, as it does somewhat in *KNM-BG 35250com*. This is most likely explained by the plastic deformation of the holotype partial skeleton highlighted elsewhere, especially at the radial notch area, which barely projects laterally (e.g., Ishida et al., 2004; Nakatsukasa et al., 2012; Takano et al., 2018; Pina et al., 2021). This trend is also shown in the combined specimen *KNM-BG 35250com* (Figure 6), in which PAB and TAB are taken from KNM-BG 35250V, suggesting that the trochlear surface area of the coronoid process is also somewhat distorted in the latter (the shaft is clearly mediolaterally compressed). On the other hand, KNM-BG 38391B falls in the *Ateles* morphospace and displays some affinities with younger and more derived (extant ape-like) extinct taxa such as *Griphopithecus* and *Hispanopithecus* (e.g., wider coronoid process; Figure 6), which might relate to the incipient presence of more derived features of the *Nacholapithecus* elbow (such as emerging traits at the radial notch associated with the enhancement of pronation-supination). This fact might correspond to the more derived distal humerus in this taxon (Takano et al., 2020; Nakatsukasa and Kunimatsu, 2009), whereby the ulnar trochlear articular surface could accommodate a wider trochlear groove of the humerus, a feature related to the enhancement of elbow stabilization when the forelimb is extended (Rose, 1988; Takano et al., 2020).

It is important to point out that most of the Mosimann variables (except PAP) and the GM16 used in this study show a degree of phylogenetic signal for both the Pagel's λ and Blomberg's K statistics. If λ is considered, most of the variables tend to conform to a Brownian motion model of evolution (λ = 1), allowing us to discard that similarities between groups are derived from homoplasy, but instead stem from close phylogenetic relatedness (Pagel, 1999). On the other hand, Blomberg's K allows us to identify the model of evolution embedded in these variables, showing that the variance is accumulated within clades and distantly related taxa resemble each other more than expected under a Brownian motion model (K < 1; Blomberg et al., 2003). Hence, given that a significant phylogenetic signal is affecting the variance of our sample, similarities between groups need to be considered within this framework and affinities may be less related to functionality. Interestingly, RPD shows one of the lowest λ values, suggesting that the shape of the radial notch might be related to the functionality of the elbow to some extent and most probably to the enhancement of pronation-supination (antipronograde behaviors) vs joint stabilization in a flexed and pronated position (quadrupeds).

Given that KNM-BG 35250C is clearly distorted, it is expected that quantitative comparisons with other *Nacholapithecus* ulnar remains highlight differences between them. This is the case of our results, in which KNM-BG 35250C displays a relatively shorter olecranon, and a deeper and narrower epiphysis than KNM-BG 38391A (Figures 2, 3B, 4A, C). Although these differences might fit within the potential range of intraspecific variation of the taxon (see a review for the proximal end of the femur in Pina et al., 2021; see also Takano et al., 2020), it is more likely that the results are affected by the reported deformation in KNM-BG 35250C. The latter displays a particularly mediolaterally compressed olecranon and a badly deformed radial notch

and, moreover, plastic deformation has been also reported for other anatomical regions of the holotype partial skeleton (Ishida et al., 2004; Nakatsukasa et al., 2012; Takano et al., 2018; Pina et al., 2021). The addition of the combined specimen to the study may help to elucidate whether the differences between KNM-BG 35250C and KNM-BG 38391A are real or just derived from the proposed deformation of the holotype specimen. When combining relatively reliable measurements, *KNM-BG 35250com* is somewhat intermediate or slightly more similar to KNM-BG 38391A in most instances. Also, *KNM-BG 35250com* departs from the majority of the sample for the PAB/TAB index, probably because PAB is underestimated due to the clear mediolateral compression affecting the specimen (especially at the shaft level). All these results confirm that plastic deformation (mainly at the most affected part, which is the radial notch area, and the general mediolateral compression of the proximal end of the ulna) is impacting the morphology of the holotype proximal ulna when analyzing the set of 16 measurements used in this study (consequently, the combined specimen also reflects this unnatural morphology). Unfortunately, proximal ulnar fragments attributed to *Ekembo* could not be included in our analyses due to its incomplete nature (e.g., NPD cannot be measured in KNM-RU 1786, and KNM-RU 2036CF lacks the olecranon process). Nonetheless, comparisons between *Ekembo* and *Nacholapithecus* have been published elsewhere (e.g., Takano et al., 2018, 2020; Nishimura et al., 2022) suggesting that the latter displays some differentiating (mostly derived) features compared with proconsulids (e.g., more anteriorly projected and broader coronoid and relatively shorter olecranon).

The proximal ulnar morphology in *Nacholapithecus* reflects the trend reported for most Miocene apes in which both the skeleton as a whole and most of their individual anatomical elements display a mixture of primitive and derived features. Some of the

traits (e.g., moderately long olecranon and non-keeled sigmoid notch) resemble those described for primitive catarrhines (Richmond et al., 1998; Ishida et al., 2004). These traits are associated with biomechanical performances related to basically quadrupedal behaviors and less specialized for pronation-supination movements (in relation to extant apes), such as arboreal quadrupedalism with generalized elbow-flexed postures (Nakatsukasa et al., 1998; Nakatsukasa and Kunimatsu, 2009; Takano et al., 2018, 2020). Nonetheless, the overall elbow in *Nacholapithecus* has been described as distinctive, already showing more derived (extant hominoid-like) features related to the stabilization of the humeroulnar joint (e.g., wide and concave superior articular surface of the coronoid process) and the performance of antipronograde behaviors such as vertical climbing, cautious climbing, and/or clambering (suspension has been tentatively ruled out on the basis of other anatomical evidence).

Our results support the previous hypothesis that *Nacholapithecus* ulnar morphology is like that of *Griphopithecus* and *Equatorius* (Figures 2-4; e.g., Takano et al., 2018) and reveal similarities with the ulna of *Hispanopithecus* too (Figure 5). Compared with extant taxa, *Nacholapithecus* shows closer morphological affinities to papionins than to non-papionin cercopithecoids and platyrrhines (e.g., relative length of the olecranon, OLP; and a relatively shallow epiphysis, SND). Nonetheless, these similarities do not mean that *Nacholapithecus* has a set of common terrestrial characters as it lacks the posteriorly retroflexed olecranon shown in *Equatorius* and papionins, while it has a more laterally facing radial notch and a wider coronoid process. Yet, such resemblances could lead one to think that *Nacholapithecus* might have some terrestrial/semi-terrestrial habits (already noted by Rose et al., 1996 on the basis of BM, sexual dimorphism, and phalanx morphology), as reported for *Equatorius* (the other member of the subfamily Equatorinae; McCrossin, 1994; McCrossin and Benefit, 1997;

Patel, Susman, Rossie & Hill, 2009), thus using terrestrial substrates more frequently than other non-Equatorinae Miocene apes like *Ekembo* (Ward, Walker, Teaford & Odhiambo, 1993). However, it is hard to think that *Nacholapithecus* was an obligate terrestrial primate when considering other anatomical features that indicate clear arboreal affinities (e.g., long pedal phalanges; Nakatsukasa and Kunimatsu, 2009).

Terrestrial features include the robustness of the ulna (e.g., relatively anteroposteriorly thick epiphysis), the relative length and retroflexion of the olecranon, and the mediolateral narrowness of the epiphysis (Rose, 1988; Nishimura et al., 2022). This complex of traits has been related to the effective leverage of the muscle triceps brachii and the reduction of the trochlear size-increasing of the radial head size (this tandem associated with preferential loading transmission through the radio-humeral joint; Richmond et al., 1988; Rose, 1993; McCrossin and Benefit, 1997; Schmitt, 1994). However, in other well-preserved anatomical areas, *Nacholapithecus* lacks additional traits clearly associated with the frequent use of the ground. For instance, *Nacholapithecus* knee morphology departs from that of terrestrial cercopithecines, usually showing a marked projection of the lateral rim of the patellar groove at the distal femur, which is also mediolaterally narrow and deep. This morphology corresponds with that of the patellar shape, since the patella is relatively long proximodistally, narrow mediolaterally, and displays a compartmentalized articular surface in this group of primates (Ward et al., 1995; Nakatsukasa et al., 2012; Pina, Almécija, Alba, O'Neill and Moyà-Solà, 2014; Pina, DeMiguel, Puigvert, Marcé-Nogué and Moyà-Solà, 2020; Pina et al., 2021). Overall, this morphology of the distal femur-patella complex helps to avoid the lateral dislocation of the patella during quadrupedal (and bipedal) movements (e.g., MacPhee and Meldrum, 2006; DeSilva et al., 2013). Therefore, it is difficult to assume that *Nacholapithecus* was a strict terrestrial quadruped, given the lack of clear

terrestrial features in other parts of the skeleton and, also, the incipient extant hominoid-like traits found in its elbow (including the proximal ulna and radius) and other anatomical elements more frequently related to arboreal antipronograde behaviors (e.g., Nakatsukasa and Kunimatsu, 2009; Takano et al., 2020; Arias-Martorell et al., 2023). Therefore, how terrestriality was integrated within the locomotor repertoire of *Nacholapithecus* remains unclear.

Conclusions

We quantify here the proximal ulnar morphology of *Nacholapithecus kerioi*, whose elbow joint has been described as joining primitive (general quadruped monkey-like) traits with derived (extant hominoid-like) features (e.g., Takano et al., 2020).

As expected, we have identified some differences between the two *Nacholapithecus* ulnae analyzed, one belonging to the holotype skeleton (KNM-BG 35250C) and another well-preserved proximal fragment (KNM-BG 38391B). These two fossils mainly differ in those variables related to the dimensions of the radial notch and the mediolateral breath of the proximal shaft, which seems to be the area most affected by plastic deformation (also underpinned by the results derived from the combined specimen *KNM-BG 35250com*). Our results, together with previous work in which the distortion of the holotype specimen was highlighted, suggest that KNM-BG 35250C does not preserve its original form and needs to be used with caution when included in comparative analysis.

Our results also support previous findings suggesting that the elbow of *Nacholapithecus* (including the ulna) is similar to those of large papionins (e.g., *Papio*) and the extinct taxon *Equatorius* (the other component of the subfamily Equatorinae) on the basis of qualitative comparisons. Although previous authors also advocated for

some affinities with *Griphopithecus* (mainly related to the configuration of the trochlear surface-radial notch complex), our analyses show that *Nacholapithecus* displays a relatively longer olecranon and a thinner sigmoid notch depth. Overall, the proximal ulnar morphology of *Nacholapithecus* indicates that some of its traits might enhance the leverage of the muscle triceps brachii and the loading through the elbow joint. These features have been related elsewhere to terrestrial quadrupedalism, however, *Nacholapithecus* lacks other traits associated with the use of this substrate, not only in the proximal ulna (e.g., retroflexion of the olecranon) but also in the rest of the skeleton. Thus, although these features are important within the elbow complex of this taxon, our results also accord with the fact that *Nacholapithecus* forelimb already displays more extant-hominoid, derived traits related to arboreal antipronograde behaviors.

Acknowledgments

The authors thank all the people involved in the numerous campaigns at the Baragoi area, their work made possible to collect a plentiful assemblage of *Nacholapithecus* and other vertebrate taxa fossil remains.

We thank Frederick Kyalo Manthi, Tom Mhukuyu, and Francis Muchemi for the access and assistance during the study of the *Nacholapithecus* specimens. We also thank Eileen Westing for access to the primate collection in the AMNH (USA) and Ursula Göhlich for access to the *Epipliopithecus* fossils in the NHMW (Austria). We thank Sergio Almécija and Salvador Moyà-Solà for providing some of the 3D ulnar models and casts used in this study.

We are grateful to the National Museums of Kenya (Earth Sciences Department) and the NACOSTI agency for permission to develop this study (NACOSTI/P/18/36012/24986). This work was funded by the JSPS International Research Fellowship (P17394 to M.P.); the European Commission under the Marie Skłodowska-Curie Individual Fellowship Programme (H2020-MSCA-IF-2018-837966 to M.P.); the postdoctoral fellowships programme Beatriu de Pinós (ref. 2022 BP 00265 to M.P.), funded by the Secretary of Universities and Research (Government of Catalonia) and by the Horizon 2020 programme of research and innovation of the European Union under the Marie Skłodowska-Curie grant agreement No 801370; the Agencia Estatal de Investigación (Spanish Ministerio de Economía y Competitividad: PROYECTO/AEI/10.13039/501100011033, MINECO/FEDER, EU), the Generalitat de Catalunya (#CLT009/18/00071 and CLT0009_22_000018), the L.S.B. Leakey Foundation (to M.P.); and the JSPS Kakenhi (16H02757 and 23K27253) and KU Core-stage Backup Program (to M.N.). This research also received support from the Synthesys Project http://synthesys3.myspecies.info/ which is financed by the European

Community Research Infrastructure Action under the FP7 (BE-TAF-3356 and AT-TAF-4689 to M.P.).

Conflict of interest

Authors declare no conflicts of interest.

Data Sharing Statement

New data derived from *Nacholapithecus* fossil remains and used in this study are included in the main text and supporting information. Further requests should be directed to the corresponding author.

References

Alba, D. M. (2012). Fossil apes from the Vallès-Penedès Basin (NE Iberian Peninsula): Phylogenetic, paleobiogeographic and paleobiological implications. *Evolutionary Anthropology, 21*, 254-269.

Alba, D. M., Moyà-Solà, S., & Almécija, S. (2011). A partial hominoid humerus from the Middle Miocene of Castell de Barberà (Vallès-Penedès Basin, Catalonia, Spain). *American Journal of Physical Anthropology*, *144*(3), 365–381.

Alba, D. M., Almécija, S., Casanovas-Vilar, I., Méndez, J. M., & Moyà-Solà, S. (2012). A partial skeleton of the fossil great ape *Hispanopithecus laietanus* from Can Feu and the mosaic evolution of crown-hominoid positional behaviors. *PloS ONE, 7*(6), e39617.

Arias-Martorell, J., Urciuoli, A., Almécija, S., Alba, D.M., Nakatsukasa, M. (2023). The radial head of the Middle Miocene ape Nacholapithecus kerioi: Morphometric affinities, locomotor inferences, and implications for the evolution of the hominoid humeroradial joint. *Journal of Human Evolution, 178,* 103345. https://doi.org/10.1016/j.jhevol.2023.103345

Arnold, C., Matthews, L.J. & Nunn, C.L. (2010). The 10kTrees website: A new online resource for primate phylogeny. *Evolutionary Anthropology, 19,* 114-118.

Begun, D. R. (1992). Phyletic Diversity and Locomotion in Primitive European Hominids. *American Journal of Physical Anthropology, 87*, 311-340.

Blomberg, S. P., Garland, T. Jr. & Ives, A. R. (2003). Testing for phylogenetic signal in comparative data: behavioral traits are more labile. *Evolution, 57,* 717-745.

Böhme, M., Spassov, N., Fuss, J., Tröscher, A., Deane, A.S., Prieto, J., Kirscher, U., Lechner, T., Begun, D.R. (2019). A new Miocene ape and locomotion in the

ancestor of great apes and humans. *Nature 575*, 489–493. https://doi.org/10.1038/s41586-019-1731-0

DeSilva, J. M., Holt, K. G., Churchill, S. E., Carlson, K. J., Walker, C. S., Zipfel, B., & Berger, L. R. (2013). The Lower Limb and Mechanics of Walking in *Australopithecus sediba*. *Science, 340*(6129). https://doi.org/10.1126/science.1232999

Drapeau, M. S. M. (2004). Functional anatomy of the olecranon process in hominoids and Plio-Pleistocene hominins. *American Journal of Physical Anthropology,* 124, 297–314. https://doi.org/10.1002/ajpa.10359

Drapeau, M. S. M. (2008). Articular morphology of the proximal ulna in extant and fossil hominoids and hominins. *Journal of Human Evolution*, *55*, 86–102. https://doi.org/10.1016/j.jhevol.2008.01.005

Farris, J. S. (1969). On the cophenetic correlation coefficient. *Systematic Biology, 18*, 279–285. https://doi.org/10.2307/2412324

Fleagle, J., Simons, E., & Conroy, G. (1975). Ape limb bone from the oligocene of Egypt. *Science*, *189*, 135–137. https://doi.org/10.1126/science.1138369

Harrison, T. (1986). A Reassessment of the Phylogenetic Relationships of *Oreopithecus bambolii* Gervais. *Journal of Human Evolution, 15*, 541-583.

Ishidal, H., Kunimatsu, Y., Nakatsukasa, M., & Nakano, Y. (1999). New Hominoid Genus from the Middle Miocene of Nachola, Kenya. *Anthropological Science, 107*, 189-191. https://doi.org/10.1537/ase.107.189

Ishida, H., Kuminatsu, Y., Takano, T., Nakano, Y., & Nakatsukasa, M. (2004). *Nacholapithecus* skeleton from the Middle Miocene of Kenya. *Journal of Human Evolution, 46*, 69-103.

Jungers, W.L., Falsetti, A.B., & Wall, C.E. (1995). Shape, relative size, and size-adjustments in morphometrics. *Yearbook of Physical Anthropologu, 38,* 137-161.

Kikuchi, Y. (2023). Body mass estimates from postcranial skeletons and implication for positional behavior in *Nacholapithecus kerioi*: Evolutionary scenarios of modern apes. *The Anatomical Record, 306,* 2466-2483. https://doi.org/10.1002/ar.25173

Kikuchi, Y., Nakatsukasa, M., Tsujikawa, H., Nakano, Y., Kunimatsu, Y., Ogihara, N., Ogihara, N., Shimizu, D., Takano, T., Nakaya, H., Sawada, Y., Ishida, H. (2018). Sexual dimorphism of body size in an African fossil ape, *Nacholapithecus kerioi*. *Journal of Human Evolution, 123*, 129-140. https://doi.org/10.1016/j.jhevol.2018.07.003

Kunimatsu, Y., Nakatsukasa, M., Shimizu, D., Nakano, Y., Ishida, H. (2019). Loss of the subarcuate fossa and the phylogeny of *Nacholapithecus*. *Journal of Human Evolution, 131*, 22-27. https://doi.org/10.1016/j.jhevol.2019.03.004

Leakey, R. E., Leakey, M. G., & Walker, A. C. (1988). Morphology of *Turkanapithecus kalakolensis* from Kenya. *American Journal of Physical Anthropology, 76*, 277-288. https://doi.org/10.1002/ajpa.1330760302

MacPhee, R. D. E., & Meldrum, J. E. F. F. (2006). Postcranial Remains of the Extinct Monkeys of the Greater Antilles, with Evidence for Semiterrestriality in *Paralouatta*. *American Museum Novitates, 2006*, 1-65.

McCrossin, M. L. (1994). Semi-terrestrial adaptations of *Kenyapithecus* [Abstract]. *American Journal of Physical Anthropology, 37*(Suppl. 18), 142-143.

McCrossin, M. L., & Benefit, B. R. (1997). On the relationships and adaptations of *Kenyapithecus*, a large-bodied hominoid from the Middle Miocene of Eastern Africa. In D. R. Begun, C. V. Ward, & M. D. Rose (Eds.), *Function, Phylogeny*

and Fossils: Miocene Hominoid Evolution and Adaptation (pp. 241-267). New York: Plenum Press.

Mosimann, J.E. (1970) Size allometry: Size and shape variables with characterizations of the lognormal and generalized gamma distributions. Journal of the American *Statistical Association, 65,* 930-945.

Nakatsukasa, M., & Kunimatsu, Y. (2009). *Nacholapithecus* and its importance for understanding hominoid evolution. *Evolutionary Anthropology: Issues, News, and Reviews, 18*, 103-119. https://doi.org/10.1002/evan.20208

Nakatsukasa, M., Yamanaka, A., Kunimatsu, Y., Shimizu, D., & Ishida, H. (1998). A newly discovered *Kenyapithecus* skeleton and its implications for the evolution of positional behavior in Miocene East African hominoids. *Journal of Human Evolution, 34*, 657-664.

Nakatsukasa, M., Kunimatsu, Y., Shimizu, D., Nakano, Y., Kikuchi, Y., & Ishida, H. (2012). Hind limb of the *Nacholapithecus kerioi* holotype and implications for its positional behavior. *Anthropological Science, 120,* 235-250.

Nishimura, A.C., Russo, G.A., Nengo, I.O., & Miller, E.R. (2022). Morphological affinities of a fossil ulna (KNM-WS 65401) from Buluk, Kenya. *Journal of Human Evolution*, *166,* 103177. https://doi.org/10.1016/j.jhevol.2022.103177

Patel, B. A., Susman, R. L., Rossie, J. B., & Hill, A. (2009). Terrestrial adaptations in the hands of *Equatorius africanus* revisited. *Journal of Human Evolution, 57*, 763-772.

Pagel, M. (1999). Inferring the historial patterns of biological evolution. *Nature, 401*, 877-884.

Pina, M., Almécija, S., Alba, D. M., O'Neill, M. C., & Moyà-Solà, S. (2014). The Middle Miocene ape *Pierolapithecus catalaunicus* exhibits extant great ape-like

morphometric affinities on its patella: inferences on knee function and evolution. *PLoS ONE, 9*(3), e91944.

Pina, M., DeMiguel, D., Puigvert, F., Marcé-Nogué, J., & Moyà-Solà, S. (2020). Knee function through finite element analysis and the role of Miocene hominoids in our understanding of the origin of antipronograde behaviours: the *Pierolapithecus catalaunicus* patella as a case study. *Palaeontology, 63*, 459-475. https://doi.org/10.1111/pala.12466

Pina, M., Kikuchi, Y., Nakatsukasa, M., Nakano, Y., Kunimatsu, Y., Ogihara, N., . . . Ishida, H. (2021). New femoral remains of *Nacholapithecus kerioi*: Implications for intraspecific variation and Miocene hominoid evolution. *Journal of Human Evolution, 155*, 102982. https://doi.org/10.1016/j.jhevol.2021.102982

Pugh, K. D. (2022). Phylogenetic analysis of Middle-Late Miocene apes. *Journal of Human Evolution, 165*, 103140. https://doi.org/10.1016/j.jhevol.2021.103140

R Core Team (2022). R: A language and environment for statistical computing. R Foundation for Statistical Computing, Vienna, Austria. URL https://www.R-project.org/

RStudio Team. (2022). RStudio: Integrated Development Environment for R. RStudio, PBC, Boston, MA URL http://www.rstudio.com/

Rein, T. R., Harrison, T., & Zollikofer, C. P. E. (2011). Skeletal correlates of quadrupedalism and climbing in the anthropoid forelimb: Implications for inferring locomotion in Miocene catarrhines. *Journal of Human Evolution*, *61*, 564–574. https://doi.org/10.1016/j.jhevol.2011.07.005

Richmond, B. G., Fleagle, J. G., Kappelman, J., & Swisher, C. C. (1998). First hominoid from the Miocene of Ethiopia and the evolution of the catarrhine elbow. *American Journal of Physical Anthropology, 105*, 257-277.

Rose, M. D. (1983). Miocene hominoid postcranial morphology. Monkey-like, ape-like, neither, or both? In R. L. Ciochon & R. S. Corruccini (Eds.), *New Interpretations of Ape and Human Ancestry* (pp. 503–516). Plenum Press.

Rose, M. D. (1988). Another look at the anthropoid elbow. *Journal of Human Evolution, 17*, 193-224.

Rose, M. D. (1997). Functional and Phylogenetic Features of the Forelimb in Miocene Hominiods. In D. R. Begun, C. Ward, & M. D. Rose (Eds.), *Function, Phylogeny, and Fossils: Miocene Hominoid Evolution and Adaptations* (pp. 79-100). New York: Plenum Press.

Rose, M. D. (1993). Functional anatomy of the elbow and forearm in primates. In D. L. Gebo (Ed.), *Postcranial Adaptation in Nonhuman Primates* (pp. 70-95). DeKalb: Northern Illinois University Press.

Rose, M. D., Nakano, Y., & Ishida, H. (1996). *Kenyapithecus* postcranial specimens from Nachola, Kenya. *African Study Monographs, Suppl. 24*, 3-56.

Ruff, C. B. (2002). Long Bone Articular and Diaphyseal Structure in Old World Monkeys and Apes. I: Locomotor Effects. *American Journal of Physical Anthropology, 119*, 305-342.

Ruff, C. B. (2003). Long Bone Articular and Diaphyseal Structure in Old World Monkeys and Apes. II: Estimation of Body Mass. *American Journal of Physical Anthropology, 120*, 16-37.

Sawada, Y., Pickford, M., Itaya, T., Makinouchi, T., Tateishi, M., Kabeto, K., Ishida, S., Ishida, H. (1998). K-Ar ages of miocene hominoidea (*Kenyapithecus* and *Samburupithecus*) from Samburu Hills, Northern Kenya. *Comptes Rendus de l'Acadèmie des Sciences - Series IIA - Earth and Planetary Science, 326*, 445-451. https://doi.org/10.1016/S1251-8050(98)80069-4

Schindelin J, Arganda-Carreras I, Frise E, Kaynig V, Longair M, Pietzsch T, Preibisch S, Rueden C, Saafeld S, Schmid B, Tinevez J-Y, White Dj, Hartenstein V, Eliceiri K, Tomancak P & Cardona A. (2012). Fiji: an open-source platform for biological-image analysis. *Nature Methods, 9*, 676-682.

Schmitt, D. (1994). Forelimb mechanics as a function of substrate type during quadrupedalism in two anthropoid primates. *Journal of Human Evolution, 26*, 441-457. http://dx.doi.org/10.1006/jhev.1994.1027

Schmitt, D. (2003). Mediolateral reaction forces and forelimb anatomy in quadrupedal primates: Implications for interpreting locomotor behavior in fossil primates. *Journal of Human Evolution*, *44*, 47–58. https://doi.org/10.1016/S0047-2484(02)00165-3

Sherwood, R. J., Ward, R. J., Hill, A., Duren, D. L., Drown, B., & Downs, W. (2002). Preliminary description of the *Equatorius africanus* partial skeleton KNM-TH 28860 from Kipsaramon, Tugen Hills, Baringo District, Kenya. *Journal of Human Evolution, 42*, 63-73.

Smith, R. J., & Jungers, W. L. (1997). Body mass in comparative primatology. *Journal of Human Evolution, 32*, 523-559.

Sokal, R. R., & Rohlf, F. J. (1962). The comparison of dendrograms by objective methods. *Taxon, 11,* 33-40. https://doi.org/10.2307/1217208

Takano, T., Nakatsukasa, M., Kunimatsu, Y., Nakano, Y., Ogihara, N., & Ishida, H. (2018). Forelimb long bones of *Nacholapithecus* (KNM-BG 35250) from the middle Miocene in Nachola, northern Kenya. *Anthropological Science, 126*, 135-149.

Takano, T., Nakatsukasa, M., Pina, M., Kunimatsu, Y., Nakano, Y., Morimoto, N., Ogihara, N., & Ishida, H. (2020). New forelimb long bone specimens of

Nacholapithecus kerioi from the Middle Miocene of northern Kenya. *Anthropological Science, 128,* 27-40. https://doi.org/10.1537/ase.200116

Urciuoli, A., & Alba, D.M. (2023). Systematics of Miocene apes: State of the art of a neverending controversy. *Journal of Human Evolution, 175,* 103309. https://doi.org/10.1016/j.jhevol.2022.103309

Ward, C. V., Walker, A., Teaford, M. F., & Odhiambo, I. (1993). Partial Skeleton of *Proconsul nyanzae* From Mfangano Island, Kenya. *American Journal of Physical Anthropology, 90*, 77-111.

Ward, C. V., Ruff, C. B., Walker, A., Teaford, F., Rose, M. D., & Nengo, I. O. (1995). Functional morphology of *Proconsul* patellas from Rusinga Island, Kenya, with implications for other Miocene-Pliocene catarrhines. *Journal of Human Evolution, 29*, 1-19.

Zapfe, H. (1960). Die Primatenfunde aus der miozänen Spaltenfüllung von Neudorf an der March (Devinská Nová Ves), Tschechoslowakei. *Schweizerische palaeontologische Abhandlungen / Mémoires Suisses de Paléontologie, 78*, 1-293.

Figure Legends

Figure 1. Linear measurements taken on the proximal ulnae sample. Except for OLP (see abbreviation definitions in Table 2), the rest of measurements were taken following Richmond et al. (1998). OLP was taken by drawing two parallel lines perpendicular to NPD (sigmoid notch proximodistal length), one crossing the most proximal point of the sigmoid notch and the other tangential to the most proximal point of the olecranon process. The distance between these two lines is recorded as OLP (defined as the length of the olecranon process, Table 2). Anterior (top left); proximal (top right); and lateral (bottom) views. Figure modified from Richmond et al. (1998).

Figure 2. Principal component analysis (PCA) plot showing PC1 and PC2. The PCA includes all 16 Mosimann variables and the geometric mean (lnGM16). The variance explained by each component is shown in parentheses. Colors represent major taxonomic groups: dark blue = great apes; light blue = hylobatids; purple = platyrrhines; dark yellow = cercopithecoids; green = extinct taxa.

Figure 3. Boxplots showing the most relevant Mosimann variables. A) ln(TAB/GM16); B) ln(PAB/GM16); C) ln(NPD/GM16); and D) ln(RPD/GM16). Vertical lines represent the median; boxes, the interquartile range, IQR (25th and the 75th percentiles); whiskers, 1.5 × IQR, and circles the outliers. Colors represent major taxonomic groups: dark blue = great apes; light blue = hylobatids; purple = platyrrhines; dark yellow = cercopithecoids; green = extinct taxa. See Table 6 for PC loadings and variable definitions in Table 2.

Figure 4. Boxplots showing the most relevant Mosimann variables. A) ln(SND/GM16); B) ln(OPML/GM16); C) ln(OLP/GM16); and D) ln(SHMN/GM16). Vertical lines represent the median; boxes, the interquartile range, IQR (25th and the 75th percentiles); whiskers, 1.5 × IQR, and circles the outliers. Colors represent major taxonomic groups: dark blue = great apes; light blue = hylobatids; purple = platyrrhines; dark yellow = cercopithecoids; green = extinct taxa. See Table 6 for PC loadings and variable definitions in Table 2.

Figure 5. Dendrogram (agglomerative hierarchical analysis, UPGMA algorithm) for PC1 and PC2 using the Mosimann variables and the geometric mean (lnGM16). CPCC = Cophenetic Correlation Coefficient. Colors represent major taxonomic groups: dark blue = great apes; light blue = hylobatids; purple = platyrrhines; dark yellow = cercopithecoids; green = extinct taxa. Nodes are numbered to better follow the result descriptions in the main text.

Figure 6. Biplot showing the relationship between PAB/GM16 vs TAB/GM (GM16 = geometric mean of the 16 variables included in this study; PAB = proximal shaft anteroposterior thickness at distal margin of radial notch; TAB = trochlear articular mediolateral breadth). Colors represent major taxonomic groups: dark blue = great apes; light blue = hylobatids; purple = platyrrhines; dark yellow = cercopithecoids; green = extinct taxa. Grey dashed line marks isometry.

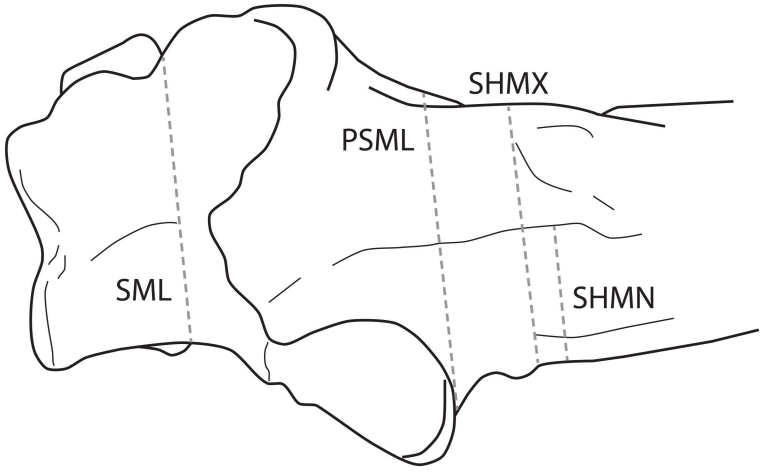
SHMX
PSML
SML
SHMN

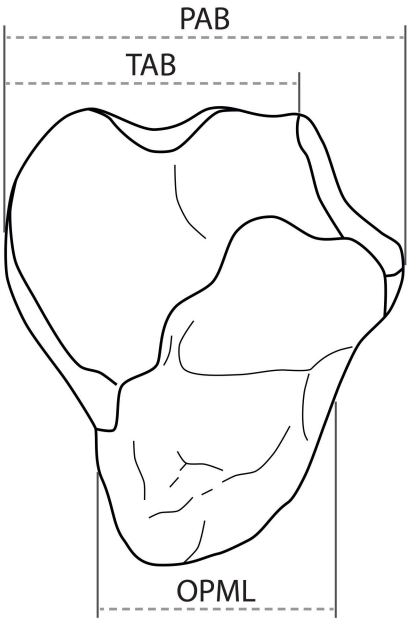
PAB
TAB
OPML

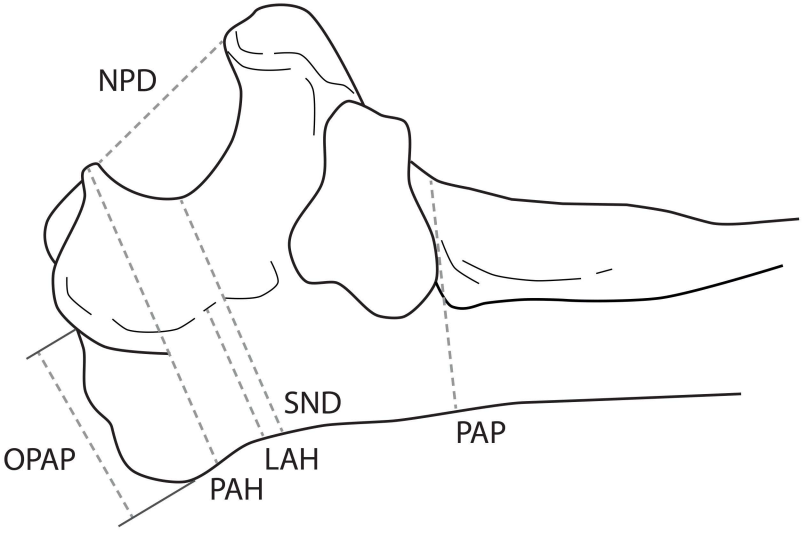
NPD
SND
PAP
OPAP
LAH
PAH

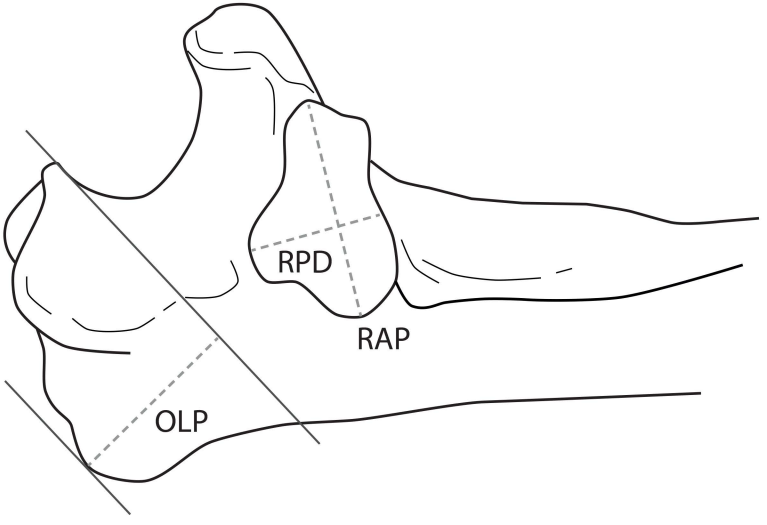
RPD
RAP
OLP

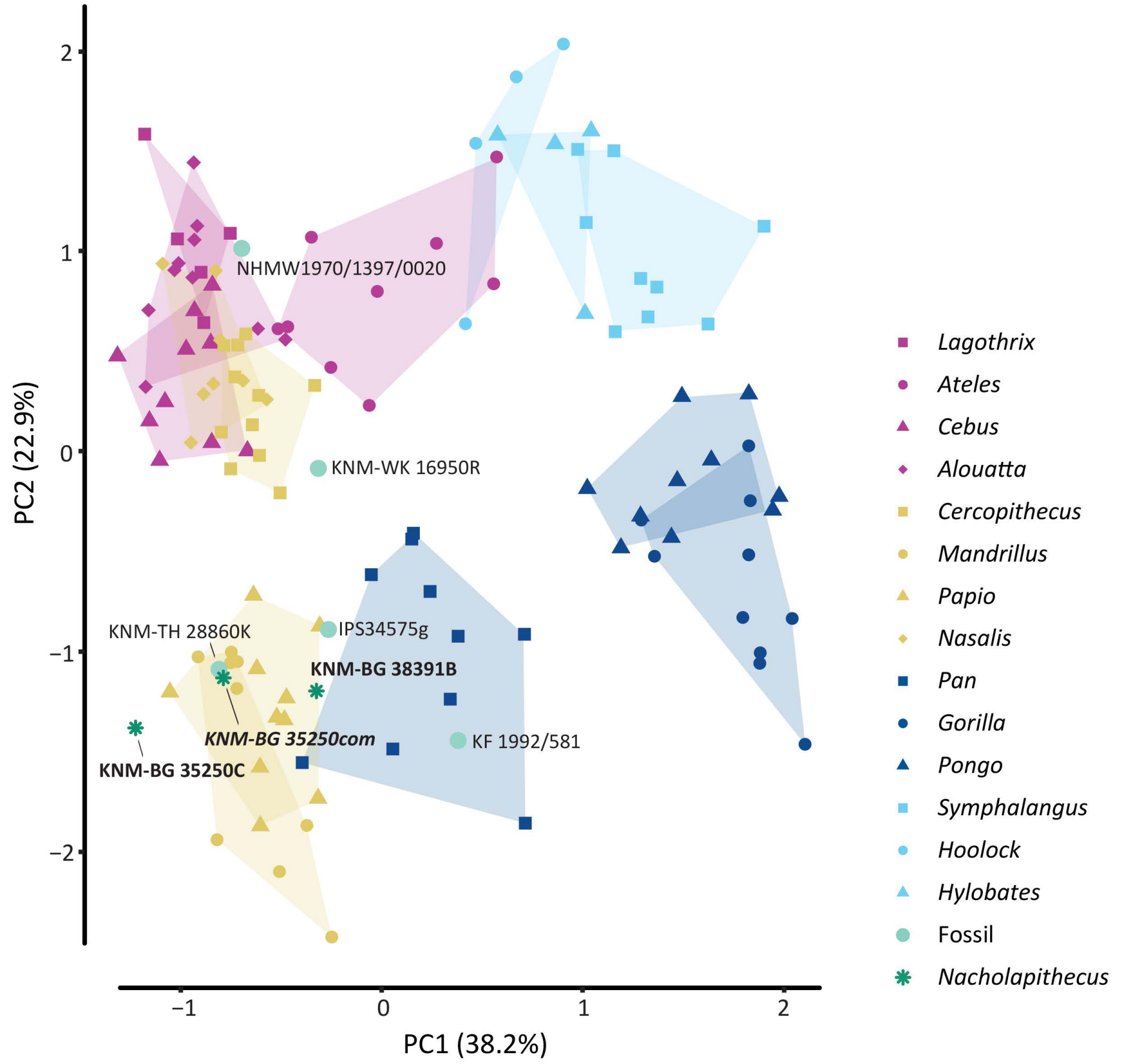
NHMW1970/1397/0020
KNM-WK 16950R
KNM-TH 28860K
IPS34575g
KNM-BG 38391B
KNM-BG 35250com
KF 1992/581
KNM-BG 35250C
PC2 (22.9%)
PC1 (38.2%)
2
1
0
−1
−2
−1
0
1
2
Lagothrix
Ateles
Cebus
Alouatta
Cercopithecus
Mandrillus
Papio
Nasalis
Pan
Gorilla
Pongo
Symphalangus
Hoolock
Hylobates
Fossil
Nacholapithecus

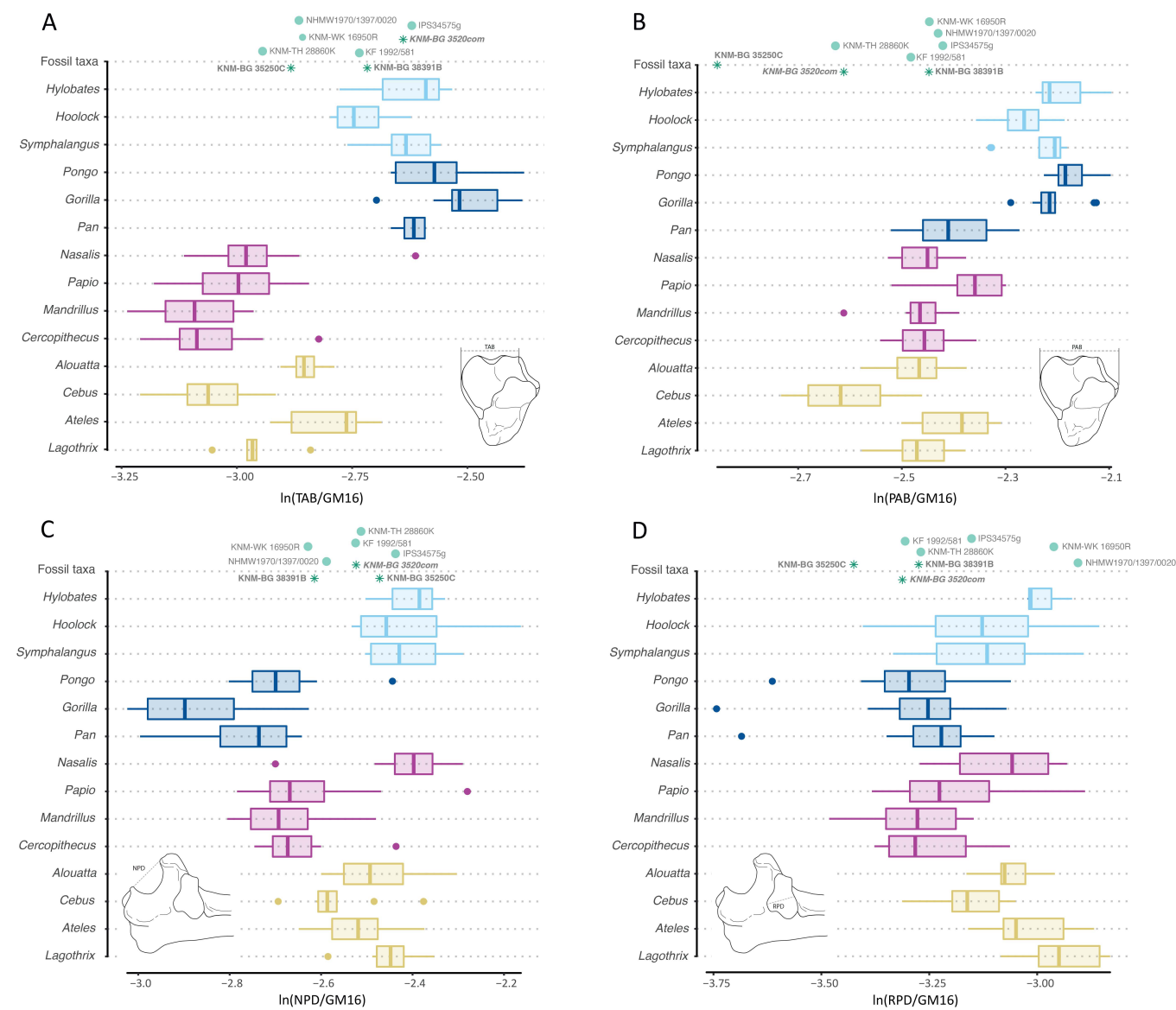
A
NHMW1970/1397/0020
IPS34575g
KNM-WK 16950R
KNM-BG 3520com
KNM-TH 28860K
KF 1992/581
KNM-BG 35250C
KNM-BG 38391B
Fossil taxa
Hylobates
Hoolock
Symphalangus
Pongo
Gorilla
Pan
Nasalis
Papio
Mandrillus
Cercopithecus
Alouatta
Cebus
Ateles
Lagothrix
TAB
−3.25
−3.00
−2.75
−2.50
ln(TAB/GM16)
B
KNM-WK 16950R
NHMW1970/1397/0020
KNM-TH 28860K
IPS34575g
KF 1992/581
KNM-BG 35250C
KNM-BG 3520com
KNM-BG 38391B
Fossil taxa
PAB
−2.7
−2.5
−2.3
−2.1
ln(PAB/GM16)
C
KNM-TH 28860K
KNM-WK 16950R
KF 1992/581
NHMW1970/1397/0020
IPS34575g
KNM-BG 3520com
KNM-BG 38391B
KNM-BG 35250C
Fossil taxa
NPD
−3.0
−2.8
−2.6
−2.4
−2.2
ln(NPD/GM16)
D
KF 1992/581
IPS34575g
KNM-TH 28860K
KNM-WK 16950R
KNM-BG 35250C
KNM-BG 38391B
NHMW1970/1397/0020
KNM-BG 3520com
Fossil taxa
RPD
−3.75
−3.50
−3.25
−3.00
ln(RPD/GM16)

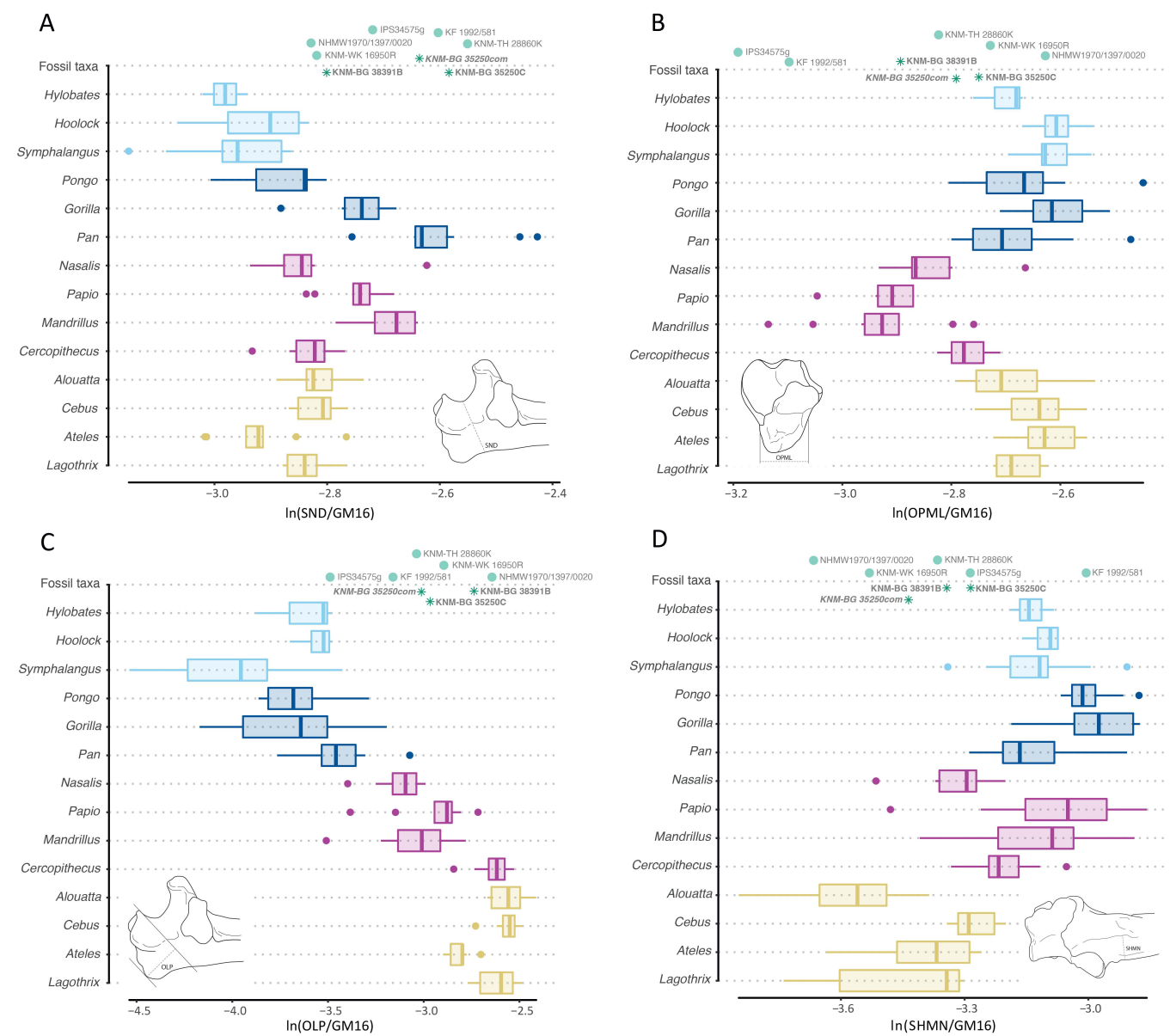
A
IPS34575g
KF 1992/581
NHMW1970/1397/0020
KNM-TH 28860K
KNM-WK 16950R
KNM-BG 35250com
KNM-BG 38391B
KNM-BG 35250C
Fossil taxa
Hylobates
Hoolock
Symphalangus
Pongo
Gorilla
Pan
Nasalis
Papio
Mandrillus
Cercopithecus
Alouatta
Cebus
Ateles
Lagothrix
SND
−3.0
−2.8
−2.6
−2.4
ln(SND/GM16)
B
KNM-TH 28860K
KNM-WK 16950R
IPS34575g
KF 1992/581
NHMW1970/1397/0020
KNM-BG 38391B
KNM-BG 35250com
KNM-BG 35250C
Fossil taxa
Hylobates
Hoolock
Symphalangus
Pongo
Gorilla
Pan
Nasalis
Papio
Mandrillus
Cercopithecus
Alouatta
Cebus
Ateles
Lagothrix
OPML
−3.2
−3.0
−2.8
−2.6
ln(OPML/GM16)
C
KNM-TH 28860K
KNM-WK 16950R
IPS34575g
KF 1992/581
NHMW1970/1397/0020
KNM-BG 35250com
KNM-BG 38391B
KNM-BG 35250C
Fossil taxa
Hylobates
Hoolock
Symphalangus
Pongo
Gorilla
Pan
Nasalis
Papio
Mandrillus
Cercopithecus
Alouatta
Cebus
Ateles
Lagothrix
OLP
−4.5
−4.0
−3.5
−3.0
−2.5
ln(OLP/GM16)
D
NHMW1970/1397/0020
KNM-TH 28860K
KNM-WK 16950R
IPS34575g
KF 1992/581
KNM-BG 38391B
KNM-BG 35250C
KNM-BG 35250com
Fossil taxa
Hylobates
Hoolock
Symphalangus
Pongo
Gorilla
Pan
Nasalis
Papio
Mandrillus
Cercopithecus
Alouatta
Cebus
Ateles
Lagothrix
SHMN
−3.6
−3.3
−3.0
ln(SHMN/GM16)

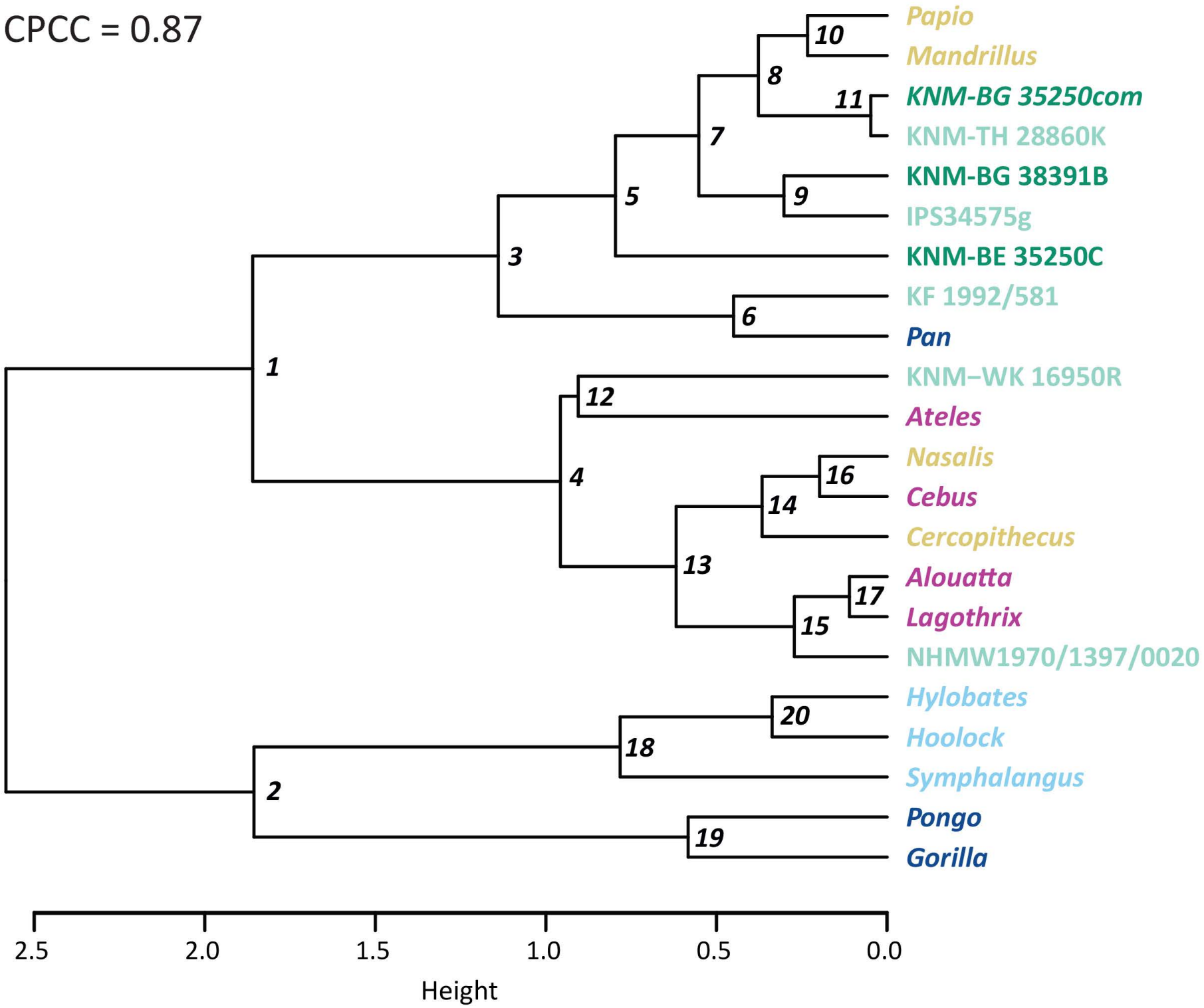
CPCC = 0.87
Papio
Mandrillus
KNM-BG 35250com
KNM-TH 28860K
KNM-BG 38391B
IPS34575g
KNM-BE 35250C
KF 1992/581
Pan
KNM–WK 16950R
Ateles
Nasalis
Cebus
Cercopithecus
Alouatta
Lagothrix
NHMW1970/1397/0020
Hylobates
Hoolock
Symphalangus
Pongo
Gorilla
1
2
3
4
5
6
7
8
9
10
11
12
13
14
15
16
17
18
19
20
2.5
2.0
1.5
1.0
0.5
0.0
Height

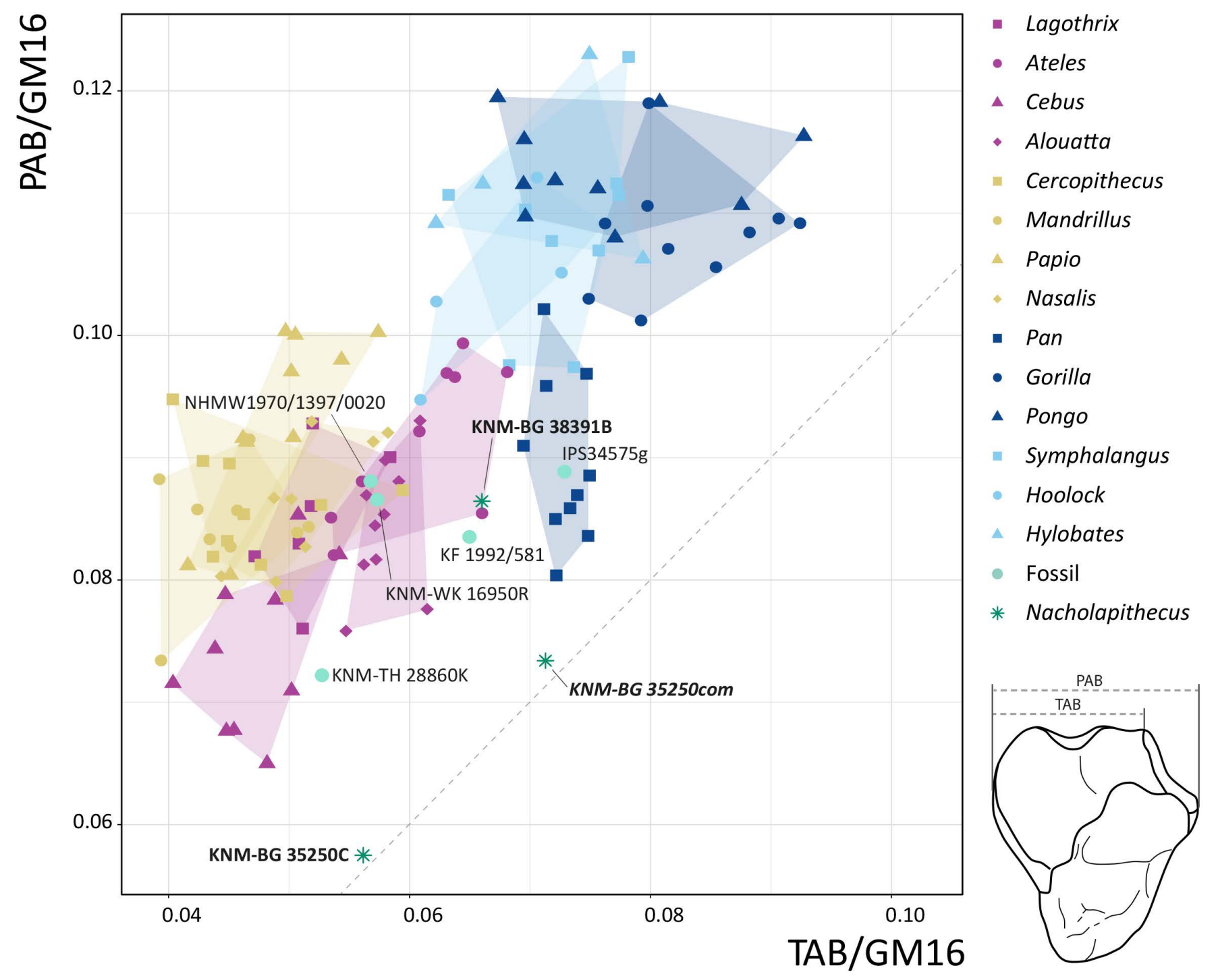
PAB/GM16
TAB/GM16
0.12
0.10
0.08
0.06
0.04
0.06
0.08
0.10
NHMW1970/1397/0020
KNM-BG 38391B
IPS34575g
KF 1992/581
KNM-WK 16950R
KNM-TH 28860K
KNM-BG 35250com
KNM-BG 35250C
Lagothrix
Ateles
Cebus
Alouatta
Cercopithecus
Mandrillus
Papio
Nasalis
Pan
Gorilla
Pongo
Symphalangus
Hoolock
Hylobates
Fossil
Nacholapithecus
PAB
TAB

Table 1. *Nacholapithecus kerioi* specimens included in this study and their respective linear measurements (in mm). See measurement illustrations, definitions and descriptions in Figure 1 and Table 2.

Accession number	Locality	Side	SML	PSML	SHMX	SHMN	NPD	OPAP	PAH	LAH	SND	RAP	RPD	PAP	PAB	TAB	OPML	OLP
KNM-BG 17824	BG-I	R	-	16.10	13.50	8.10	-	-	-	-	?16.9	9.50	-	19.80	-	-	-	-
KNM-BG 35250V	BG-K	R	13.10	12.90	12.00	7.60	-	-	-	15.60	17.00	9.60	8.60	20.80	17.30	16.80	14.30	-
KNM-BG 35250C	BG-K	L	11.20	11.50†	11.20†	8.40†	18.90	19.20	24.40	14.50	16.90	8.60	7.30†	20.80†	12.90†	12.60†	14.40	11.59
KNM-BG 35250com‡			11.20	12.90	12.00	7.60	18.90	19.20	24.40	14.50	16.90	8.60	8.60	20.80	17.30	16.80	14.40	11.59
KNM-BG 37352	BG-K	L	-	16.70	13.10	10.10	-	-	-	-	-	9.20	6.60	21.30	21.90	19.60	-	-
KNM-BG 38391B	BG-K	R	11.90	14.90	13.70	8.30	17.20	19.60	25.30	12.90	14.30	6.70	8.90	17.20	20.30	15.50	13.00	15.14
KNM-BG 38610B	BG-K	R	-	-	14.30	11.10	7.50	-	-	-	-	8.50	11.50	21.20	11.60	15.80	-	-

†, tentative measurements; ‡, specimen that combines measurements from both KNM-BG 35250V and KNM-BG 35250C (see text for further explanation).

Table 2. Definition of the linear measurements used in this work (after Richmond et al., 1998, except for OLP). See also Figure 1. All measurements were taken in mm.

Abbreviation	Description
SML	Sigmoid notch mediolateral width
PSML	Proximal shaft mediolateral width at distal margin of radial notch
SHMN	Minimum mediolateral width of shaft anterior to brachialis insertion
SHMX	Maximum mediolateral width of shaft including brachialis insertion
NPD[†]	Sigmoid notch proximodistal length from proximal to distal beaks
OPAP	Olecranon process anteroposterior thickness
PAH	Proximal articular anteroposterior thickness at anconeal process
LAH	Lateral anteroposterior articular thickness from posterior border of lateral articular surface to posterior border of shaft
SND	Sigmoid notch depth; minimum antero-posterior thickness of sigmoid notch
RAP	Radial notch anteroposterior thickness
RPD	Radial notch proximodistal length
PAP	Proximal shaft anteroposterior thickness at distal margin of radial notch
PAB	Proximal articular mediolateral breadth of radial notch and trochlea
TAB[‡]	Trochlear articular mediolateral breadth
OPML	Olecranon process mediolateral breadth
OLP	Olecranon process length from the most proximal point of the sigmoid notch

[†], NPD = UTSI in Ruff (2002); [‡], TAB = UTML in Ruff (2002).

Table 3. Extant and extinct specimens used for comparisons with *Nacholapithecus* ulnae.

Taxon	F	M	U	Total
Lagothrix lagotricha	2	3	1	6
Ateles sp.	4	3	1	8
Cebus sp.	2	7	1	10
Alouatta seniculus	1	4	5	10
Cercopithecus sp.	4	6		10
Mandrillus sp.		6	3	9
Papio sp.	1	4	5	10
Nasalis larvatus	1	6	1	8
Pan troglodytes	3	7		10
Gorilla sp.	3	7		10
Pongo pygmaeus	4	2	4	10
Symphalangus syndactylus	6	2	1	9
Hoolock hoolock	3		1	4
Hylobates sp.	1	2	1	4
Epipliopithecus vindobonensis (NHMW1970/1397/0020)				1
Equatorius africanus (KNM-TH 28860K)				1
Turkanapithecus kalakolensis (KNM-WK 16950R)				1
Griphopithecus darwini (KF 1992/581)				1
Hispanopithecus laietanus (IPS34575g)				1

F, females; M, males; U, unknown sex.

Table 4. Linear parameter values used to calculate the body mass (BM, in kg) of KNM-BG 38391B. Estimations are based on the ulnar trochlear surface area (UTSA), following published BM prediction equations for catarrhines (including cercopithecoids and hominoids) and hominoids alone (see text for further explanation).

KNM-BG 38391B	**NPD**	**TAB**	**UTDP**	**UTSA**	**BM**	**SEE**	**CI 50%**	**CI 95%**
Hominoids	23.61	16.52	10.97	584.93	26.49	1.11	24.61-28.52	21.17-33.15
Catarrhines					29.89	1.19	26.55-33.64	22.01-40.58

NPD, superoinferior height of the sigmoid notch (mm); TAB, mediolateral breadth of the trochlear articular surface (mm); UTDP, depth of the trochlear notch (mm); UTSA, ulnar trochlear surface area (mm^2); BM, body mass (kg); SEE, standard error of estimate; CI, confidence interval (kg).

Table 5. Phylogenetic signal for the Mosimann variables and the lnGM16 (GM16) represented by the Blomberg's K and Pagel's λ metrics and their respective *p-values*. Each Mosimann variable -ln(Variable/GM16)- is represented by the abbreviation of its correspondent linear variable (see Table 2). NS, no significative.

Variables	**K**	***p-value***	**λ**	***p-value***
GM16	0.471	<0.05	0.974	<0.05
SML	0.902	<0.05	1.000	<0.05
PSML	0.122	NS	0.708	<0.05
SHMX	0.339	<0.05	0.911	<0.05
SHMN	0.316	<0.05	0.868	<0.05
NPD	0.370	<0.05	0.948	<0.05
OPAP	0.887	<0.05	0.999	<0.05
PAH	0.117	NS	0.913	<0.05
LAH	0.123	NS	0.869	<0.05
SND	0.216	<0.05	0.953	<0.05
RAP	0.234	<0.05	0.878	<0.05
RPD	0.128	NS	0.484	<0.05
PAP	0.022	NS	0.540	NS
PAB	0.510	<0.05	0.950	<0.05
TAB	0.776	<0.05	0.881	<0.05
OPML	0.582	<0.05	0.950	<0.05
OLP	0.131	NS	0.887	<0.05

Table 6. PC (principal component) loadings for PC1-PC3 based on proximal ulnar Mosimann variables -ln(Variable/GM16)- represented by the abbreviation of the correspondent linear variable defined in Table 2, and the lnGM16 (GM16). Variables with the highest positive and negative loadings in each axis are highlighted in bold.

Variables	PC1	PC2	PC3
GM16	0.205	-0.361	0.213
SML	0.309	0.140	0.236
PSML	0.289	-0.185	-0.307
SHMX	0.243	-0.253	-0.275
SHMN	0.234	-0.236	**-0.414**
NPD	-0.130	**0.335**	-0.191
OPAP	-0.308	-0.006	-0.153
PAH	-0.299	-0.228	0.037
LAH	-0.197	-0.277	0.143
SND	-0.072	**-0.392**	0.346
RAP	0.057	0.316	-0.258
RPD	-0.103	**0.337**	0.099
PAP	-0.260	-0.126	-0.067
PAB	**0.324**	0.080	-0.034
TAB	**0.321**	0.042	**0.364**
OPML	0.164	0.252	**0.365**
OLP	**-0.324**	0.017	0.093

Supporting Information [SI]

New quantitative analyses of the *Nacholapithecus kerioi* proximal ulna confirm morphological affinities with *Equatorius* and large papionins

Marta Pina[1,2*], Masato Nakatsukasa[3]

[1] *South Bank Applied BioEngineering Research (SABER), School of Engineering, London South Bank University, London SE1 0AA, UK.*

[2§] *Institut Català de Paleontologia Miquel Crusafont, Universitat Autònoma de Barcelona, c/ Columnes s/n, Campus de la UAB, 08193 Cerdanyola del Vallès, Barcelona, Spain.* marta.pina@icp.cat

[3] *Laboratory of Physical Anthropology, Graduate School of Science, Kyoto University, Kyoto 606-8502, Japan.* nakatsuk@anthro.zool.kyoto-u.ac.jp

*Corresponding author:

E-mail address: marta.pina@icp.cat (M. Pina)

§ Present institution

Figure S1. Principal component analysis (PCA) plots (A and B) and dendrograms (C and D) showing A, C) PC1 vs PC3 and B, D) PC2 vs PC3. The analyses include all 16 Mosimann variables and the geometric mean (lnGM16). The variance explained by each component in the PCAs is shown between parentheses. Dendrograms were performed using the UPGMA algorithm in the agglomerative hierarchical analysis of the PC scores. CPCC = Cophenetic Correlation Coefficient. Colors represent major taxonomic groups: dark blue = great apes; light blue = hylobatids; purple = platyrrhines; dark yellow = cercopithecoids; green = extinct taxa; dark green = *Nacholapithecus*.

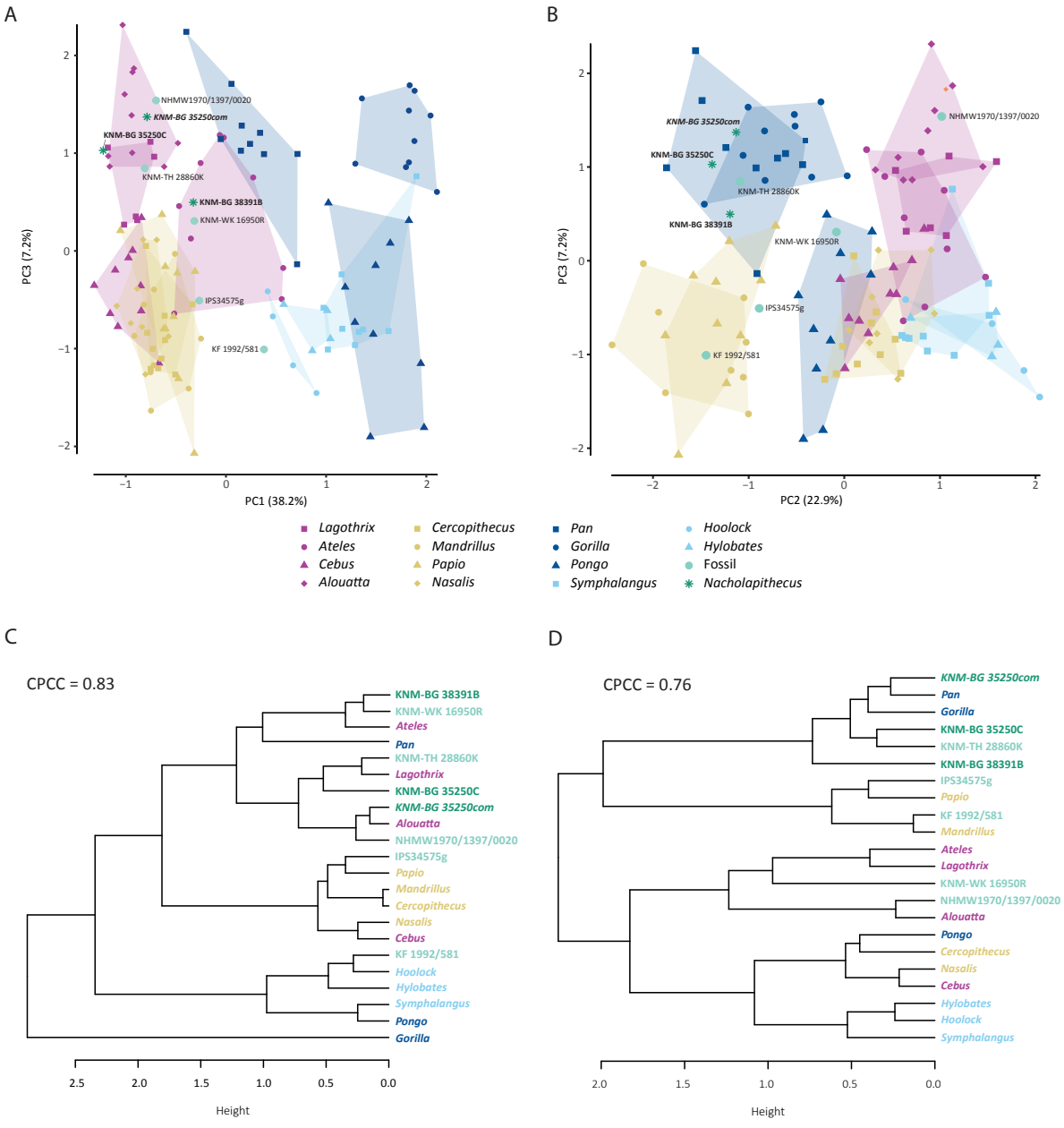

Table S1. Post-hoc pairwise comparisons (*p-values*) among extant anthropoids for PC1-PC3 scores (Kruskal-Wallis test) and PC pairs (permutation MANOVA). *p-values*: NS, no significant differences; *, $p < 0.05$; **, $p < 0.005$; ***, $p < 0.001$.

		Kruskal-Wallis test			Permutation MANOVA		
Genera		PC1	PC2	PC3	PC1-PC2	PC1-PC3	PC2-PC3
Ateles	*Alouatta*	***	NS	**	*	*	*
Cebus	*Alouatta*	NS	**	***	*	*	*
Cercopithecus	*Alouatta*	*	**	***	*	*	*
Gorilla	*Alouatta*	***	***	NS	*	*	*
Hoolock	*Alouatta*	**	NS	*	*	*	*
Hylobates	*Alouatta*	**	NS	*	*	*	*
Lagothrix	*Alouatta*	NS	NS	*	NS	*	*
Mandrillus	*Alouatta*	*	***	***	*	*	*
Nasalis	*Alouatta*	NS	*	***	*	*	*
Pan	*Alouatta*	***	***	NS	*	*	*
Papio	*Alouatta*	*	***	***	*	*	*
Pongo	*Alouatta*	***	***	***	*	*	*
Symphalangus	*Alouatta*	***	NS	***	*	*	*
Cebus	*Ateles*	***	*	NS	*	*	*
Cercopithecus	*Ateles*	**	**	**	*	*	*
Gorilla	*Ateles*	***	***	*	*	*	*
Hoolock	*Ateles*	*	NS	*	*	*	NS
Hylobates	*Ateles*	**	NS	*	NS	*	NS
Lagothrix	*Ateles*	**	NS	NS	*	*	NS
Mandrillus	*Ateles*	**	***	**	*	*	*
Nasalis	*Ateles*	***	NS	*	*	*	*
Pan	*Ateles*	NS	***	*	*	*	*
Papio	*Ateles*	*	***	*	*	*	*
Pongo	*Ateles*	***	***	*	*	*	*
Symphalangus	*Ateles*	***	NS	*	*	*	*
Cercopithecus	*Cebus*	***	NS	*	*	*	NS
Gorilla	*Cebus*	***	***	***	*	*	*
Hoolock	*Cebus*	**	*	NS	*	*	*
Hylobates	*Cebus*	**	*	NS	*	*	*
Lagothrix	*Cebus*	NS	*	*	*	*	*
Mandrillus	*Cebus*	**	***	NS	*	*	*
Nasalis	*Cebus*	NS	NS	NS	NS	NS	NS
Pan	*Cebus*	***	***	***	*	*	*
Papio	*Cebus*	**	***	NS	*	*	*
Pongo	*Cebus*	***	**	NS	*	*	*
Symphalangus	*Cebus*	***	**	NS	*	*	*
Gorilla	*Cercopithecus*	***	***	***	*	*	*
Hoolock	*Cercopithecus*	**	**	NS	*	*	*
Hylobates	*Cercopithecus*	**	**	NS	*	*	*
Lagothrix	*Cercopithecus*	*	**	**	*	*	*
Mandrillus	*Cercopithecus*	NS	***	NS	*	NS	*
Nasalis	*Cercopithecus*	*	NS	NS	*	*	NS

Pan	*Cercopithecus*	***	***	***	*	*	*
Papio	*Cercopithecus*	NS	***	NS	*	NS	*
Pongo	*Cercopithecus*	***	*	NS	*	*	*
Symphalangus	*Cercopithecus*	***	***	NS	*	*	*
Hoolock	*Gorilla*	**	**	*	*	*	*
Hylobates	*Gorilla*	**	**	*	*	*	*
Lagothrix	*Gorilla*	**	**	NS	*	*	*
Mandrillus	*Gorilla*	***	**	***	*	*	*
Nasalis	*Gorilla*	***	***	***	*	*	*
Pan	*Gorilla*	***	NS	NS	*	*	NS
Papio	*Gorilla*	***	*	***	*	*	*
Pongo	*Gorilla*	NS	*	***	*	*	*
Symphalangus	*Gorilla*	*	***	***	*	*	*
Hylobates	*Hoolock*	NS	NS	NS	NS	*	NS
Lagothrix	*Hoolock*	*	NS	*	*	*	*
Mandrillus	*Hoolock*	**	*	NS	*	*	*
Nasalis	*Hoolock*	*	*	NS	*	*	*
Pan	*Hoolock*	NS	**	*	*	*	*
Papio	*Hoolock*	**	**	NS	*	*	*
Pongo	*Hoolock*	**	**	NS	*	*	*
Symphalangus	*Hoolock*	**	NS	NS	*	*	NS
Lagothrix	*Hylobates*	*	NS	*	*	*	*
Mandrillus	*Hylobates*	**	*	NS	*	*	*
Nasalis	*Hylobates*	*	*	NS	*	*	*
Pan	*Hylobates*	*	**	*	*	*	*
Papio	*Hylobates*	**	**	NS	*	*	*
Pongo	*Hylobates*	*	**	NS	*	*	*
Symphalangus	*Hylobates*	*	NS	NS	NS	NS	NS
Mandrillus	*Lagothrix*	*	**	**	*	*	*
Nasalis	*Lagothrix*	NS	*	**	NS	*	*
Pan	*Lagothrix*	**	**	NS	*	*	*
Papio	*Lagothrix*	*	**	*	*	*	*
Pongo	*Lagothrix*	**	**	*	*	*	*
Symphalangus	*Lagothrix*	**	NS	*	*	*	*
Nasalis	*Mandrillus*	NS	***	NS	*	NS	*
Pan	*Mandrillus*	***	NS	***	*	*	*
Papio	*Mandrillus*	NS	NS	NS	NS	NS	NS
Pongo	*Mandrillus*	***	***	NS	*	*	*
Symphalangus	*Mandrillus*	***	***	NS	*	*	*
Pan	*Nasalis*	***	***	**	*	*	*
Papio	*Nasalis*	*	***	NS	*	*	*
Pongo	*Nasalis*	***	**	NS	*	*	*
Symphalangus	*Nasalis*	***	*	NS	*	*	*
Papio	*Pan*	***	NS	***	*	*	*
Pongo	*Pan*	***	***	**	*	*	*
Symphalangus	*Pan*	***	***	***	*	*	*
Pongo	*Papio*	***	***	NS	*	*	*
Symphalangus	*Papio*	***	***	NS	*	*	*
Symphalangus	*Pongo*	NS	***	NS	*	NS	*